UNCLASSIFIED

MARTIN MARIETTA ENERGY SYSTEMS LIBRARIES
3 4456 0361026 0

CENTRAL RESEARCH LIBRARY
DOCUMENT COLLECTION

ORNL-2137
Physics cy. 4

SPATIAL DISTRIBUTION OF ELECTRON DEPTH DOSE IN ALUMINUM

F. N. Huffman

CENTRAL RESEARCH LIBRARY
DOCUMENT COLLECTION
LIBRARY LOAN COPY
DO NOT TRANSFER TO ANOTHER PERSON
If you wish someone else to see this document, send in name with document and the library will arrange a loan.

OAK RIDGE NATIONAL LABORATORY
OPERATED BY
UNION CARBIDE NUCLEAR COMPANY
A Division of Union Carbide and Carbon Corporation
UCC
POST OFFICE BOX P · OAK RIDGE, TENNESSEE

UNCLASSIFIED

Printed in USA. Price 45 cents. Available from the

Office of Technical Services
U. S. Department of Commerce
Washington 25, D. C.

LEGAL NOTICE

This report was prepared as an account of Government sponsored work. Neither the United States, nor the Commission, nor any person acting on behalf of the Commission:

A. Makes any warranty or representation, express or implied, with respect to the accuracy, completeness, or usefulness of the information contained in this report, or that the use of any information, apparatus, method, or process disclosed in this report may not infringe privately owned rights; or

B. Assumes any liabilities with respect to the use of, or for damages resulting from the use of any information, apparatus, method, or process disclosed in this report.

As used in the above, "person acting on behalf of the Commission" includes any employee or contractor of the Commission to the extent that such employee or contractor prepares, handles or distributes, or provides access to, any information pursuant to his employment or contract with the Commission.

Unclassified ORNL-2137

Contract No. W-7405-eng-26

HEALTH PHYSICS DIVISION

SPATIAL DISTRIBUTION OF ELECTRON DEPTH DOSE IN ALUMINUM

Fred N. Huffman

Date Issued

AUG 1 1956

Oak Ridge National Laboratory
Operated by
Union Carbide Nuclear Company
A Division of Union Carbide and Carbon Corporation
Post Office Box P
Oak Ridge, Tennessee

Unclassified

MARTIN MARIETTA ENERGY SYSTEMS LIBRARIES

3 4456 0361026 0

ORNL-2137
Physics
TID-4500 (11th ed.)

INTERNAL DISTRIBUTION

1. C. E. Center
2. Biology Library
3. Health Physics Library
4-5. Central Research Library
6. Reactor Experimental Engineering Library
7-26. Laboratory Records Department
27. Laboratory Records, ORNL R.C.
28. A. M. Weinberg
29. L. B. Emlet (K-25)
30. J. P. Murray (Y-12)
31. J. A. Swartout
32. E. H. Taylor
33. E. D. Shipley
34. K. Z. Morgan
35. M. L. Nelson
36. W. H. Jordan
37. S. J. Cromer
38. C. P. Keim
39. J. H. Frye, Jr.
40. G. E. Boyd
41. R. S. Livingston
42. S. C. Lind
43. F. L. Culler
44. A. H. Snell
45. A. Hollaender
46. M. T. Kelley
47. T. A. Lincoln
48. A. S. Householder
49. C. S. Harrill
50. C. E. Winters
51. D. W. Cardwell
52. J. A. Lane
53. E. E. Anderson
54. D. D. Cowen
55. R. A. Charpie
56. C. E. Clifford
57. M. J. Skinner
58. R. R. Dickison
59. F. N. Huffman
60. ORNL - Y-12 Technical Library, Document Reference Section

EXTERNAL DISTRIBUTION

61. R. F. Bacher, California Institute of Technology
62. G. E. Thoma, USAF
63. Division of Research and Development, AEC, ORO
64-766. Given distribution as shown in TID-4500 under Physics category (300 copies - OTS)

DISTRIBUTION PAGE TO BE REMOVED IF REPORT IS GIVEN PUBLIC DISTRIBUTION

TABLE OF CONTENTS

I. Statement of the Problem 5

II. The Spencer Theory of Electron Penetration 6

III. Sample Calculation of 50 kev Spatial Distribution 16

IV. Theory of Triple Plate Ionization Chamber 36

V. Description of Equipment 48

A. Accelerator 48

B. Triple Plate Ionization Chamber 48

C. Differential Pumping 53

D. Beam Positioning 56

E. Auxiliary Equipment 58

VI. Treatment of Data 63

A. Sample Calculation 63

B. Estimation of Error 66

VII. Comparison of Experiment with Theory 69

VIII. Comparison with Other Experiments 73

IX. Summary of Findings and Conclusions 74

Bibliography 77

LIST OF TABLES

I. Stopping Powers and Corresponding Residual Ranges for Electrons Calculated from the Bethe Formula 17

II. Table of Adjusted Stopping Powers 22

III. Tabulation of $(d_\ell + p + 1)$ Values 26

IV. Residual Range Moment Lattice for 50 kev 27

LIST OF FIGURES

1. Reciprocal Stopping Power as a Function of Electron Energy . . 19

2. Residual Range as a Function of Electron Energy 20

3. 57 kev Theoretical Distribution and Experimental Points . . . 37

4. 80 kev Theoretical Distribution and Experimental Points . . . 38

5. 100 kev Theoretical Distribution and Experimental Points . . . 39

6. 126.5 kev Theoretical Distribution and Experimental Points . . 40

7. Sketch of Theoretical Conditions for Measuring Forward Distribution 41

8. Sketch of Theoretical Conditions for Measuring Backscattered Distribution 41

9. Sketch of Analogous Experimental Conditions for Measuring Forward Distribution 41

10. Sketch of Analogous Experimental Conditions for Measuring Backscattered Distribution 41

11. Cross Sectional View of Triple Plate Ion Chamber 43

12. Photograph of Triple Plate Ion Chamber 44

13. Typical Plot of Incremental Current vs Pressure 47

14. Schematic Diagram of Apparatus 49

15. Photograph of Apparatus 50

16. Cross Sectional View of "Tee" Chamber 55

17. Cross Sectional View of "Positioner" 57

18. Electron Gun Power Supply 59

19. Photograph of Assembled Apparatus 62

20. Ionization Chamber Plateau 64

21. Normalized, Theoretical, Spatial Distributions as a Function of Penetration Depth 71

22. Normalized, Theoretical, Spatial Distributions as a Function of Penetration Depth 72

23. Percent Maximum Ionization vs Depth in g/cm^2 Aluminum Curves . 75

I. STATEMENT OF THE PROBLEM

The problem herein discussed is a study of the spatial distribution of electron energy dissipation in aluminum by electrons in the energy range 50 to 125 kev. The measurements were made with an electron accelerator and a triple plate ionization chamber of unique design. The spatial distributions as a function of incident energy are compared with the recent theory of L. V. Spencer.

Spencer has considered the problem of the energy dissipation of an electron beam in an infinite medium under the combined influences of scattering and slowing down. Many contributions have been made toward understanding simpler situations, in which one or another effect is neglected, but Spencer has made the first complete calculation of electron spatial distributions taking into account both energy loss and direction changes.

The primary contribution of this investigation is a measurement of energy dissipation under conditions corresponding to those assumed in Spencer's theory. Similar experiments have been made, but are unsatisfactory for checking Spencer's theory because of the lack of an adequate backscattering plate needed to approximate an infinite medium. In addition, the work described herein represents the first attempt to make an absolute measurement of dose inasmuch as previous experiments have measured the distribution only in terms of percent of maximum ionization.

II. THE SPENCER THEORY OF ELECTRON PENETRATION

Previous treatments of electron penetration have assumed in general either that scattering takes place without energy loss or that energy loss occurs with no dependence on scattering. Such approximations are adequate for absorbers which are thin compared to the range of the electrons, but theories based on these approximations fail to give even qualitatively correct results when applied to deep penetrations. Spencer[1] is the first to develop a theory of electron penetration to the point of numerical application considering both scattering and energy loss of a parallel beam originating in an infinite, homogeneous medium. If $I(r,\theta,z)dz\, d\Omega$ is the flux of electrons making angles between θ and $\theta + d\theta$ with the normal to the source plane, having residual ranges between r and r + dr and crossing a unit spherical probe at a distance z from the source plane, the flux change in going from a distance z to z + dz is given by

$$\left[I(z\ dz,\theta,r - dr) - I(z,\theta,r)\right] d\Omega\, dz = dz\, d\Omega\, dr \int d\Omega'\, N\sigma(r,\Theta) \left\{I(r,\theta',z) - I(r,\theta,z)\right\} + (2\pi)^{-1}\, \delta(z)dz\ \delta(r - r_o)dr\ \delta(\cos\theta - 1)\, d\Omega \tag{1}$$

Here, $2\pi\sigma(r,\Theta)\sin\Theta\, d\Theta$ is the cross section per atom for deflecting an electron with residual range r through an angle between Θ and $\Theta + d\Theta$. N is the number of atoms per gram and $r_o = r(T_o)$.

---

[1] L. V. Spencer, Phys. Rev. 98, 1597 (1955).

It is assumed that an electron source is located at the plane $z = 0$ and emits monoenergetic electrons in the direction $\theta = 0$, i.e., perpendicular to the source plane. Expanding the left member of the equation above, one obtains

$$- \frac{\partial I}{\partial r} + \cos\theta \frac{\partial I}{\partial z} = \int d\Omega' \, N\sigma(r, \Theta) \left\{ I(r,\theta',z) - I(r,\theta,z) \right\}$$

$$+ (2\pi)^{-1} \, \delta(z) \, \delta(r - r_o) \, \delta(\cos\theta - 1) \tag{2}$$

The relation between the residual true range r and the kinetic energy of the electrons is given by the expression below which may be integrated to give the residual range.

$$r(T) = \int_o^T dT \left(\frac{dT}{dr} \right)^{-1} \tag{3}$$

The distance parameters may be rescaled, taking $r_o = r(T_o)$ as unit and defining $t = (r/r_o)$, $x = (z/r_o)$, and $S(t, \Theta) = r_o N\sigma(r, \Theta)$. I and S are then integrated over spherical harmonics and Eq. (2) is transformed into a linked system of differential equations involving the terms of $S(t)$ and $I(t,x)$. The equation is then multiplied by x^n and integrated from -1 to +1 where

$$I_{\ell n}(t) = \int_{-1}^{1} x^n I_\ell(t,x)dx \tag{4}$$

The diffusion Eq. (2) becomes

$$-\frac{\partial I_{\ell n}}{\partial t} + S_\ell(t) I_{\ell n}(t) = n(2\ell + 1)^{-1}\left\{(\ell+1) I_{\ell+1,n-1}(t) + \ell I_{\ell-1,n-1}(t)\right\} + \delta_{no}\,\delta(t-1) \tag{5}$$

For low Z materials, the McKinley-Feshbach relativistic nuclear scattering cross section may be used and the corresponding S_ℓ is

$$S_\ell\left[t(T)\right] = (Z+1)(3N_A\phi_o Z/4A)(1+\epsilon)T^{-1}(T+2)^{-1}\beta^{-2}$$

$$\times\left\{C_\ell + 2\pi\alpha\beta\ell - (\beta^2 + \pi\alpha\beta)\sum_{i=1}^{\ell} i^{-1}\right\} r_o \tag{6}$$

Here, N_A is Avogadro's number, T is the kinetic energy in mc^2 units, $\alpha = Z/137$, $\beta = v/c$ and $\phi_o = 8\pi e^4/3m^2c^4$. ϵ represents a correction due to inelastic deflections and is given by Fano[2] as

---

[2] U. Fano, Phys. Rev. 93, 117 (1954).

$$\epsilon = (Z + 1)^{-1} \; n(4\eta)^{-1} \left\{ 5 - \ln \left[0.16 \, Z^{-2/3} \, (1 + 3.33\alpha/\beta) \right] \right\} \tag{7}$$

where η is the screening constant calculated by Moliere,

$$\eta = \frac{1}{4} \left[\frac{Z^{1/3}}{0.885(137)} \right]^2 T^{-1}(T + 2)^{-1} \times \left[1.13 + 3.76\alpha^2 \, (T+1)^2 \times T^{-1}(T+2)^{-1} \right] \tag{8}$$

The numbers C are:

$$C_o = 0$$

$$C = \ln(1 + \eta^{-1}) - (1 + \eta)^{-1}$$

$$C_{\ell+1} = (2 + \ell^{-1})(1 + 2\eta)C_\ell - (1 + \ell^{-1})C_{\ell-1} - (2 + \ell^{-1})(1 + \eta)^{-1} \tag{9}$$

Spencer demonstrates that if the source energy is less than about 1 mc^2, an approximate expression agrees well with the S_ℓ's:

$$S_\ell(t) = \frac{d_\ell}{t} \tag{10}$$

where the constants d_ℓ are evaluated at t = 1.

The formal solution of the differential equations (5) has been given by Lewis[3], but the numerical evaluation of the integral is feasible

---

[3] H. W. Lewis, Phys. Rev. 78, 526 (1950).

only for $n < 4$. Spencer avoids this difficulty by writing the transport equation in terms of integrals of the $I_{\ell n}(t)$ which are easier to calculate. The solution of Eq. (5) is obtained by multiplying by t^{p+1} and integrating over the range $0 \leq t \leq 1$. When $I^{p}_{\ell n}$ is defined as

$$I^{p}_{\ell n} = \int_{0}^{1} t^{p} I_{\ell n}(t)\, dt, \tag{11}$$

the solution is given by the system of equations

$$I^{p}_{\ell n} = \frac{n}{(d_{\ell} + p + 1)} \left\{ \frac{\ell + 1}{2\ell + 1} I^{p+1}_{\ell+1,n-1} + \frac{\ell}{2\ell + 1} I^{p+1}_{\ell-1,n-1} \right\}$$

$$+ \delta_{no} (d_{\ell} + p + 1)^{-1} \tag{12}$$

The numbers $I^{p}_{\ell o}$ now constitute the knowns and $I^{p}_{\ell n}$ may be calculated from them.

The energy dissipation distribution is given by

$$J(x) = \int_{0}^{1} I_{o}(t,x) \left(\frac{dT}{dt} \right) dt \tag{13}$$

and has the spatial moments

$$J_n = \int_0^1 I_{on}(t) \left(\frac{dT}{dt}\right) dt \tag{14}$$

It should be noted that the stopping power used here should be that of the detecting material (i.e., ion chamber gas).

If the stopping power dT/dt is fitted with the expression,

$$\frac{dT}{dt} = A_o t^{-1/2} + A_1 t^{1/2} + A_2 t^{3/2} \tag{15}$$

the spatial moments, J_n, become:

$$J_n = A_o I_{on}^{-1/2} + A_1 I_{on}^{1/2} + A_2 I_{on}^{3/2} \tag{16}$$

Since only a finite number of energy dissipation spatial moments can be calculated, the extrapolation of the distribution from a few moments may be carried out only if the trend of the highest order spatial moments obtained can be shown to have the correct asymptotic behavior at deep penetrations. Using the method of Wick,[4] Spencer has

---

[4] G. C. Wick, Phys. Rev. 75, 738 (1949).

shown that the energy dissipation distribution should be of the form

$$f(x) = (1 - x)^{-3/2} \exp\left[\frac{-A}{1 - x}\right] \qquad \text{near } x = 1 \tag{17}$$

Here, A is the asymptotic constant. The logarithms of the numbers $I_{on}^{-1/2}$, $I_{on}^{1/2}$, and $I_{on}^{3/2}$ should plot as straight lines again $\sqrt{n + 1}$.

Spencer has discussed the construction of a distribution from a knowledge of its moments and has found that a "function fitting" method can be used to advantage in problems of x-ray and electron penetration. The distribution is represented by a sum of terms:

$$J(x) = \sum_i \alpha_i F^{\gamma}(\beta_i, x) \tag{18}$$

where the $F^{\gamma}(\beta_i, x)$ is given for the parallel beam by

$$F^{\gamma}(\beta_i, x) = \beta_i^{-1}(1 - x/\beta_i)^{\gamma} \exp\left[\frac{-Ax}{\beta_i - x}\right], \quad 0 \leq x \leq \beta_i \tag{19}$$

$$= 0, \; x > \beta_i$$

Moments taken of the above equation yield

$$J_n = \sum_i \alpha_i F_n^{\gamma}(\beta_i) = \sum_i \alpha_i \beta_i^n \omega_n^{\gamma} \tag{20}$$

where

$$\omega_n^{\gamma} = \int_0^1 (1 - y)^{\gamma} \exp\left[\frac{-Ay}{1 - y}\right] y^n \, dy \tag{21}$$

The best asymptotic trend is given by $\gamma = -3/2$, and Spencer has found the asymptotic value ($n >> 1$),

$$\omega_n^{-3/2} = \left(\frac{\pi}{A}\right)^{1/2} e^{A/2} \exp\left\{-\left[4A(n + 1/4 + A/12)\right]^{1/2}\right\} \tag{22}$$

The asymptotic constant A in the equation above may be found by iteration of the equation below:

$$\ln \frac{J_n}{J_{n+2}} = (4A)^{1/2} \left\{\left[(n + 2 + 1/4) + A/12\right]^{1/2} - \left[(n + 1/4) + A/12\right]^{1/2}\right\} \tag{23}$$

Although $\gamma = -3/2$ gives the best asymptotic fit, Spencer uses $\gamma = 0$ for distributions in Al and Au and $\gamma = 1$ for Be so that the distributions will superpose without "bumps."

The integral of ω_n^o has been evaluated and gives a recursion expression for these moments.

$$\omega_n^o = A^{-1}\left\{n\,\omega_{n-1}^o - 2(n + 1)\,\omega_n^o + (n + 2)\,\omega_{n+1}^o\right\}, \quad n > 0 \tag{24}$$

$$\omega_n^o = 1 - A\, e^A \left\{ - E_i(-A) \right\} \quad , \; n = 0 \tag{25}$$

where E_i is an exponential integral. For large n, the asymptotically correct expression for ω_n^o is

$$\omega_n^o = (n + 1 + A/12)^{-1}\, e^{A/2} \left[4A(n + 1 + A/12)\right]^{1/2} \; L_1 \left[4A(n + 1 + A/12)\right]^{1/2} \tag{26}$$

$L_1(y) = yK_1(y)$ where K_1 is the modified Bessel function of the second kind of order one.

To obtain the ω_n^o, Eq. (26) is solved for two successive large moments (e.g., 21 and 20) and the recursion relation (Eq. 24) is worked backwards to find ω_o^o. All ω_o^o are then multiplied by a number such that the ω_o^o calculated above agrees with the value obtained from Eq. (25).

The Eqs. (20) are divided into two sets, one for even n and one for odd n. This procedure simplifies the algebra and gives an estimate of the accuracy of the approximation since the two component distributions should become asympotically the same. The equations to be solved are:

$$\sum_i \alpha_i \beta_i^n = \frac{J_n}{\omega_n^o} , \qquad n = 0, 2, 4 \ldots.$$

$$\sum_i \alpha_i \beta_i^n = \frac{J_n}{\omega_n^o} , \qquad n = 1, 3, 5, \ldots. \tag{27}$$

To the first of these systems is added the equation

$$\sum \alpha_i \beta_i^{-2} = A^{-1} \left(\frac{d}{dt}\right) \frac{dT}{dt}\bigg|_{t = 1} \tag{28}$$

which guarantees the known slope change at $x = 0$. To the latter set is added

$$\sum \alpha_i \beta^{-1} = \frac{dT}{dt}\bigg|_{t = 1} \tag{29}$$

to give the known discontinuity. From asymptotic considerations, $\beta_2 = 1$ in both systems. The equations are solved simultaneously and $\overset{\text{even } n}{J(x)}$ and $\overset{\text{odd } n}{J(x)}$ are evaluated by the relation,

$$J(x) = \sum_i \frac{\alpha_i}{\beta_i} e^{-(Ax/\beta_i - x)} \tag{30}$$

Then,

$$J(x) = \frac{\overset{\text{even } n}{J(|x|)} + \operatorname{sgn} x \, \overset{\text{odd } n}{J(|x|)}}{2} \tag{31}$$

III. CALCULATION OF 50 KEV SPATIAL DISTRIBUTION

A sample calculation is given below for the case of 50 kev electrons absorbed in aluminum, assuming that the ionization is to be measured in a parallel plate air cavity placed in the medium.

At least six figures are carried throughout the calculation for reasons of "internal consistency" even though input data and final result are correct to only three figures at best.

Wherever it appears, the energy is expressed in mc^2 units. Usually, however, electron energy is given in terms of $t = r/r_o$, where r_o is the total range measured along an electron track and given by an integration of the Bethe stopping power expression and r is the residual range, i.e., the distance an electron still has to traverse at any given energy.

Because the energy parameter, t, is so basic to the theory, the calculation may well begin with a determination of the dependence of t on energy. The Bethe formula[5] is given by

$$-\frac{dT}{\rho\, dy} = \frac{2\pi N_A e^4 Z}{mv^2 A}\left[\ln \frac{mv^2 T}{2I^2(1-\beta^2)} - (2\sqrt{1-\beta^2} - 1 + \beta^2)\ln 2 + 1 - \beta^2 + \frac{1}{8}(1-\sqrt{1-\beta^2})^2\right]$$

---

5 H. A. Bethe, HANDBUCH DER PHYSIK 24, Part 1, p 491, Verlag Julius Springer, Berlin, 1933.

The symbols are defined as

I = average ionization potential of an atom,

T = kinetic energy of the electron (total energy minus rest energy),

e = charge of electron,

Z = atomic number of the absorbing matter,

$\beta = v/c$,

ρ = density in g/cm^3,

A = atomic weight

m = rest mass of electron

y = distance along electron track

Spencer has given a tabulation of stopping powers and residual ranges for various materials and electron energies in his paper and Table I, given here, is an abstract from Spencer's table of the data relevant to this study.

Table I

Stopping Powers and Corresponding Residual Ranges for Electrons Calculated from the Bethe Formula

Mev	Air		Aluminum	
	Stopping power $mc^2/(g/cm^2)$	Residual range g/cm^2	Stopping power $mc^2/(g/cm^2)$	Residual range g/cm^2
0.01	38.80	0.000285	33.25	0.000339
0.03	16.67	0.00199	14.625	0.00230
0.05	11.42	0.00490	10.101	0.00559
0.07	9.011	0.00880	8.008	0.00999
0.10	7.127	0.01619	6.362	0.01830
0.20	4.843	0.05074	4.356	0.05684

The r_o values are found by integrating with a polar planimeter the plot of $(dT/\rho\, dy)^{-1}$ vs T as shown in Fig. 1. Next, a graph of r vs T is plotted as in Fig. 2. t is given by the r at T divided by the r_o at T_o, that is, the range corresponding to the incident electron energy.

The stopping power occurs in the theory as dT/dt and this may be obtained from $dT/\rho\, dy$ in the following way. If y denotes distance along the electron track, then

$$r + \rho y = r_o$$

$$dr + \rho\, dy = 0$$

$$-\frac{dT}{\rho\, dy} = \frac{dT}{dr} = \frac{1}{r_o}\,\frac{dT}{d(r/r_o)} = \frac{1}{r_o}\,\frac{dT}{dt}$$

Hence

$$\frac{dT}{dt} = -\, r_o\left(\frac{dT}{\rho\, dy}\right)$$

Because the ionization is measured in an air cavity, one must multiply the above stopping power by the ratio

$$\frac{(\text{stopping power})_{air}}{(\text{stopping power})_{Al}}$$

UNCLASSIFIED
ORNL-LR-DWG. 14866

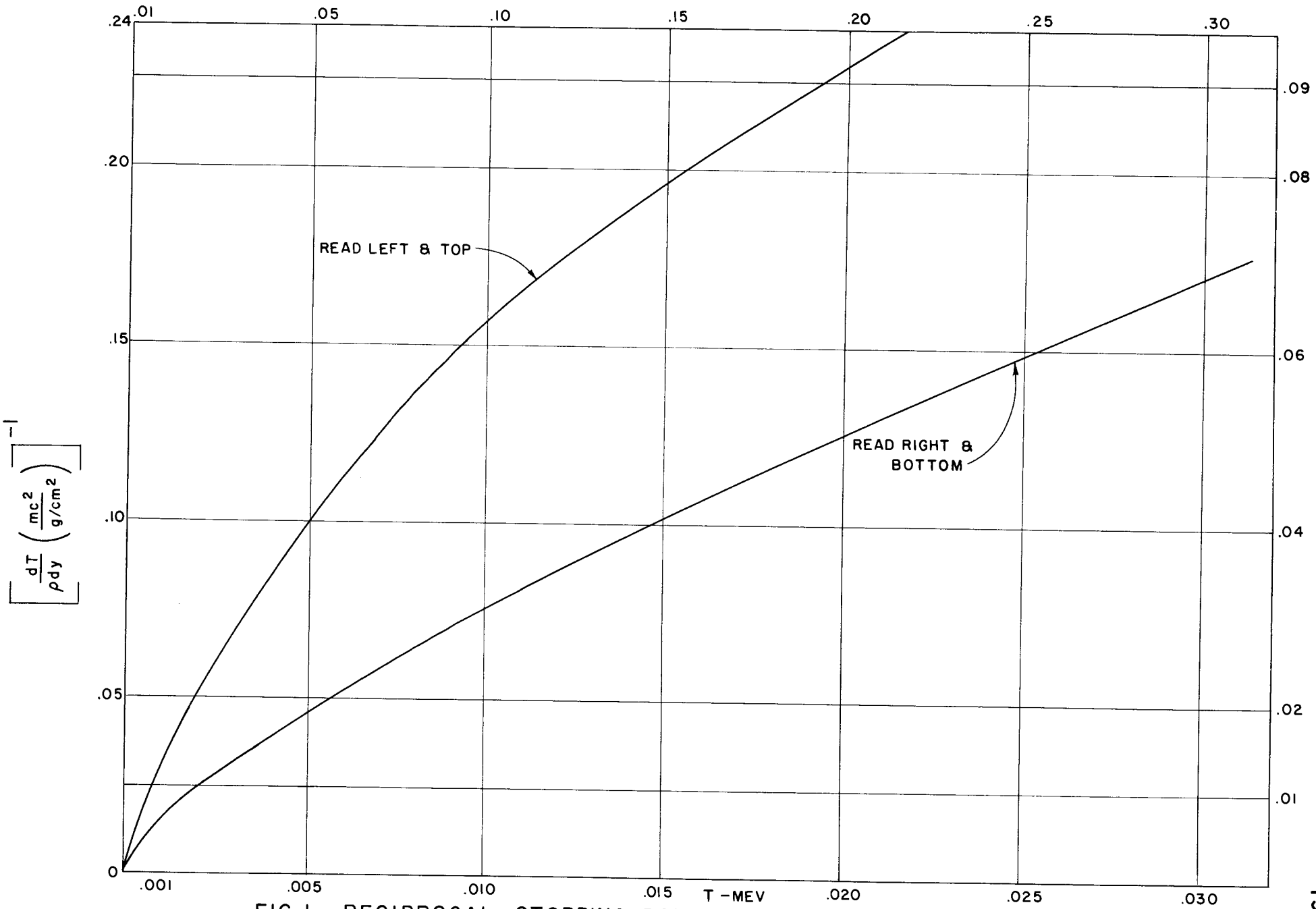

FIG. 1 - RECIPROCAL STOPPING POWER AS A FUNCTION OF ELECTRON ENERGY

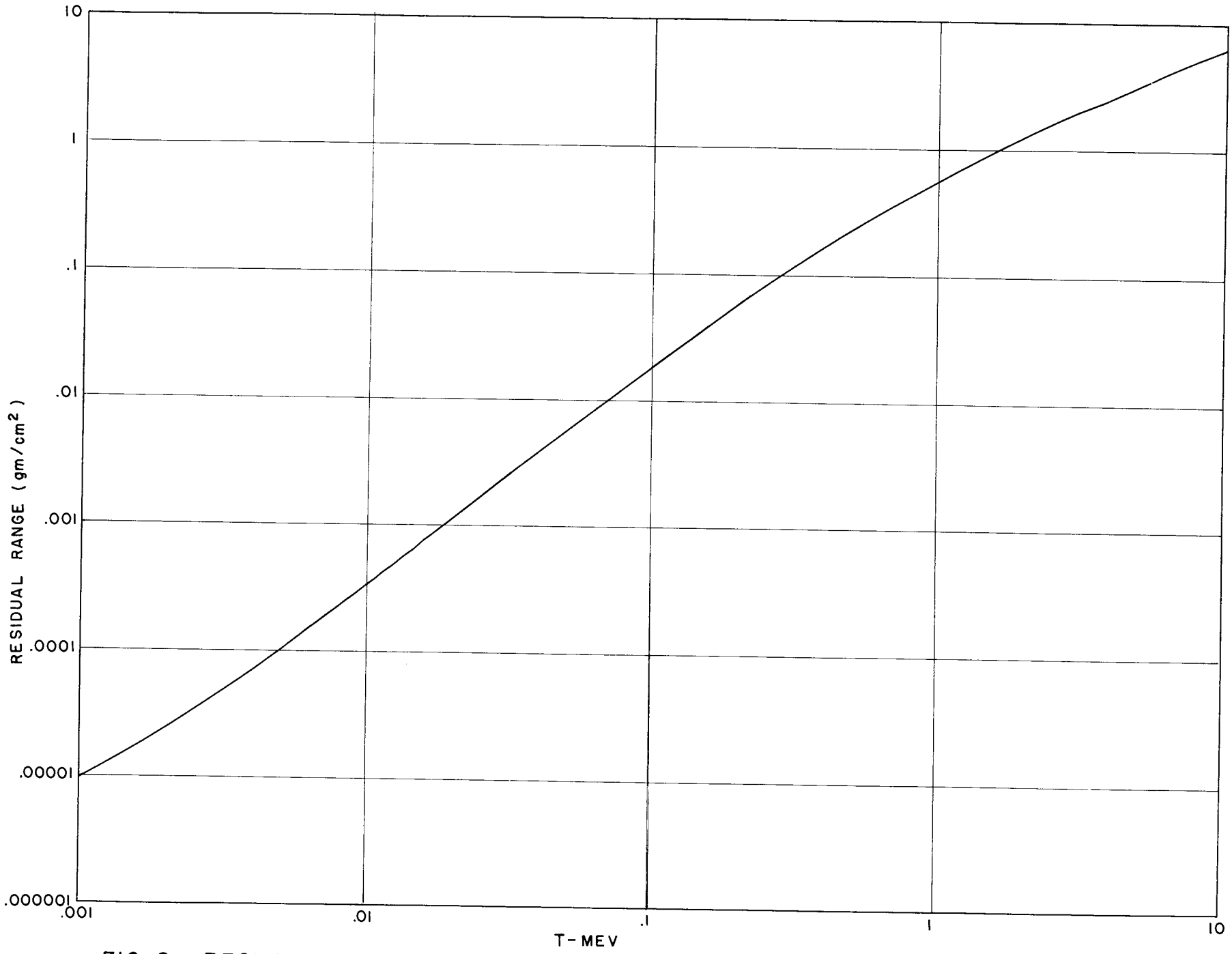

FIG. 2 - RESIDUAL RANGE AS A FUNCTION OF ELECTRON ENERGY

UNCLASSIFIED
ORNL-LR-DWG. 14867

in accordance with the Bragg-Gray principle. Then,

$$\left(\frac{dT}{dt}\right)_{corr} = \left(\frac{dT}{\rho\, dy}\, r_o\right)_{Al} \frac{(dT/\rho\, dy)_{Air}}{(dT/\rho\, dy)_{Al}} = (r_o)_{Al} \left(\frac{dT}{\rho\, dy}\right)_{Air}$$

Table II gives the adjusted stopping powers for 50 kev.

The corrected stopping power must be fitted with the expression

$$\frac{dT}{dt} = A_o t^{-1/2} + A_1 t^{1/2} + A_2 t^{3/2}$$

A least squares fit was attempted but proved impractical. An an alternative the fit was made at three values of t at approximately $t = 1$, $t = 1/2$, and $t = 0.1$. This requires solving three simultaneous equations to determine A_o, A_1 and A_2.

Table II

Table of Adjusted Stopping Powers

E (Mev)	r_o g/cm^2	t r/r_o	$(r_o)_{Al}(dT/\rho\, dy)_{Air}$
0.050	0.00559	1.00000	0.06384
0.040	0.00380	0.67985	0.07519
0.030	0.00230	0.411449	0.09319
0.020	0.00115	0.205725	0.1266
0.010	0.000347	0.062075	0.2169
0.007	0.0001896	0.0339177	0.2868
0.005	0.000108	0.0193202	0.3734
0.003	0.0000464	0.0083005	0.5601
0.001	0.0000095	0.0016995	------

An an example,

For t = 1.00000,

$$0.06384 = A_o + A_1 + A_2$$

For t = 0.411449,

$$0.09319 = 1.558985\ A_o + 0.641443\ A_1 + 0.263921\ A_2$$

For t = 0.062075,

$$0.21690 = 4.017633\ A_o + 0.249149\ A_1 + 0.015466\ A_2$$

$$A_o = 0.052762$$

$$A_1 = 0.021222$$

$$A_2 = -\ 0.010144$$

Next the quantity $S_\ell \left[t(T)\right]$ must be evaluated. For aluminum, a suitable expression is

$$S_\ell \left[t(T)\right] = (Z + 1)\left(3\, N_A\, \phi_o \frac{Z}{4A}\right) (1 + \epsilon)T^{-1}(T + 2)^{-1}\, \beta^{-2}$$

$$\times \left\{ C_\ell + 2\pi\alpha\, \beta\ell - (\beta^2 + \pi\alpha\beta) \sum_{i=1}^{\ell} i^{-1} \right\} r_o$$

For energies less than about 1 mc^2 the dependence of the S_ℓ's may be approximated by the expression $S_\ell(t) = d_\ell/t$. This representation makes possible far less laborious methods of solution than direct numerical or analytical integration. d_ℓ is evaluated at $t = 1$.

Some of the numerical values for this equation at 50 kev and for aluminum follow:

$T = 0.097847\ mc^2$

$\eta = 6.049 \times 10^{-4}$

$\alpha = 0.09489051$

$\beta = 0.412685$

$\epsilon = -0.0945244$

$\phi_o = 6.68 \times 10^{-25}$

$C_o = 0$ $\quad C_1 = 6.4116$ $\quad C_2 = 16.26009$

$C_3 = 28.58344$ $\quad C_4 = 42.72551$ $\quad C_5 = 58.27080$

$C_6 = 74.88161$ $\quad C_7 = 92.29710$

$S_1 = 1.87641$ $\quad S_5 = 17.34552$

$S_2 = 4.80933$ $\quad S_6 = 22.30072$

$S_3 = 8.48662$ $\quad S_7 = 24.49577$

$S_4 = 12.70725$

The system of equations

$$I_{\ell n}^{p} = \frac{n}{(d_\ell + p + 1)} \left\{ \frac{(\ell + 1)}{(2\ell + 1)} I_{\ell+1,n-1}^{p+1} + \frac{\ell}{2\ell + 1} I_{\ell-1,n-1}^{p+1} \right\}$$

$$+ \delta_{no} (d_\ell + p + 1)^{-1}$$

may now be computed. The Kronecker delta function, δ_{no}, has the property of being zero for all n other than zero, and the value of 1 when n = 0. For n = 0 the linkage term vanishes and $I_{\ell o}^{p} = (d_\ell + p + 1)^{-1}$. These numbers now constitute the knowns and from them the $I_{\ell 1}^{p}$ may be obtained, which in turn yield $I_{\ell 2}^{p}$, and so on. The calculation is simplified if made in lattice form with n + p = m(1/2) heading the rows and ℓ the columns. For reasons which appear later, m takes on all odd integer value from -1 to n, and a table is calculated for each value of m as

in Table IV.

Before constructing the lattice, it is convenient to tabulate the quantity, $(d_\ell + p + 1)$, from $\ell = 0$ to $\ell = 7$ vs $p + 1/2 = 0$ to $p + 1/2 = 9$ as in Table III.

Table III

Tabulation of $(d_\ell + p + 1)$ Values

$(p + 1/2)$ \ ℓ	0	1	2	3	4	5	6	7
0	0.50000							
1	1.50000	3.37641						
2	2.50000	4.51641	7.30933					
3	3.50000	5.32641	8.30933	11.98662				
4	4.50000	6.37641	9.30933	12.98662	17.20705			
5	5.50000	7.37	10.90	13.9	18.2	22.84552		
6	6.50000	8.37	11.30	14.9	19.2	23.8	28.80072	
7	7.50000	9.37	12.30	15.9	20.2	24.8	29.8	34.99577
8	8.50000	10.37	13.30	16.9	21.2	25.8	30.8	35.9
9	9.50000	11.37	14.30	17.9	22.2	26.8	31.8	36.9

Table IV

Residual Range Moment Lattice for 50 kev

n	p + 1/2 \ ℓ	0	1	2	3	4
0	0	2.00000				
0	1	6.66667^{-1}	2.96173^{-1}			
1	0	5.92346^{-1}				
0	2	4.00000^{-1}	2.28498^{-1}	1.35811^{-1}		
1	1	1.52332^{-1}	6.65030^{-2}			
2	0	2.66012^{-1}				
0	3	2.85714^{-1}	1.87744^{-1}	1.20347^{-1}	8.34264^{-2}	
1	2	7.50976^{-2}	4.00943^{-2}	1.71223^{-2}		
2	1	5.34591^{-2}	2.14895^{-2}			
3	0	1.29537^{-1}				
0	4	2.22222^{-1}	1.56828^{-1}	1.07419^{-1}	7.70023^{-2}	5.81157^{-2}
1	3	4.48080^{-2}	2.73519^{-2}	1.31098^{-2}	6.61118^{-2}	
2	2	2.18815^{-2}	1.08198^{-2}	4.0791^{-3}		
3	1	2.16396^{-2}	8.89689^{-3}			
4	0	7.11751^{-2}				

Note: Powers of ten are written as superscripts. That is, $6.66667^{-1} = 6.66667 \times 10^{-1}$.

This table is continued through $(p + 1/2) = 9$ and $\ell = 7$, giving I_{On}^{p} values listed in Table IV, continued.

Table IV, cont.

n	p + 1/2	$\ell = 0$
0	5	1.81818^{-1}
1	4	3.01260^{-2}
2	3	1.12264^{-2}
3	2	7.65878^{-3}
4	1	1.01343^{-2}
5	0	4.05754^{-2}
0	6	1.53846^{-1}
1	5	2.17060^{-2}
2	4	6.64159^{-3}
3	3	3.47145^{-3}
4	2	3.14112^{-3}
5	1	5.07330^{-3}
6	0	2.46992^{-2}
0	7	1.33333^{-1}
1	6	1.64078^{-2}
2	5	4.28058^{-3}
3	4	1.84306^{-3}
4	3	1.27033^{-3}
5	2	1.40500^{-3}
6	1	2.74497^{-3}
7	0	1.53937^{-2}

n	p + 1/2	$\ell = 0$
0	8	1.17647^{-1}
1	7	1.28497^{-2}
2	6	2.93066^{-3}
3	5	1.07888^{-3}
4	4	7.30649^{-4}
5	3	5.00114^{-4}
6	2	8.11289^{-4}
7	1	1.51546^{-3}
0	9	1.05265^{-1}
1	8	1.03413^{-2}
2	7	2.09905^{-3}
3	6	6.35002^{-4}
4	5	3.26573^{-4}
5	4	2.13802^{-4}
6	3	2.29011^{-4}
7	2	3.33990^{-4}

The numbers listed in Table IV for which p = - 1/2, 1/2, and 3/2 are combined with A_o, A_1, and A_2 as follows to yield the moments of the energy dissipation distribution.

$$J_n = A_o I_{on}^{-1/2} + A_1 I_{on}^{1/2} + A_2 I_{on}^{3/2}$$

$J_1 = 0.115614407$

$J_2 = 0.033734360$

$J_3 = 0.014947868$

$J_4 = 0.007216118$

$J_5 = 0.003938547$

$J_6 = 0.002234253$

$J_7 = 0.000840975$

Next, the asymptotic constant A must be determined. A simple iteration of the equation below will serve the purpose.

$$\ell n \frac{J_n}{J_{n+2}} = (4A)^{1/2} \left\{ \left[(n + 2 + 1/4) + A/12 \right]^{1/2} - \left[(n + 1/4) + A/12 \right]^{1/2} \right\}$$

For J_4 and J_6, A = 1.506 gives agreement to four figures.

$\gamma = 0$ is chosen because $F_n^o(\beta, x)$ superpose smoothly and the corresponding numbers ω_n^o are calculated. Then, two successive large ω_n^o, say ω_{21}^o and ω_{20}^o are calculated using the equation

$$\omega_n^o = (n + 1 + A/12)^{-1} e^{A/2} L_1 \left[4A(n + 1 + A/12)\right]^{1/2}$$

$$L_1 = y\, K_1(y)$$

where K_1 is the modified Bessel function of the second kind of order one.[6]

$$\omega_{21}^o = 4.08346536 \times 10^{-6}$$

$$\omega_{20}^o = 5.50621886 \times 10^{-6}$$

Lower moments are obtained by working the recursion equation (Eq. 24) below backwards.

$$\omega_{n-1}^o = \frac{\omega_n(A + 2n + 2) - \omega_{n+1}(n + 2)}{n}$$

$\omega_{19}^o = 0.00000748586599$

$\omega_{18}^o = 0.00001026725040$

$\omega_{17}^o = 0.00001421670414$

$\omega_{16}^o = 0.00001988939595$

$\omega_{15}^o = 0.00002814326363$

$\omega_{14}^o = 0.00004032323066$

$\omega_{13}^o = 0.00005858082050$

$\omega_{12}^o = 0.0000864336330$

$\omega_{11}^o = 0.0001297760018$

$\omega_{10}^o = 0.000198763157$

$\omega_9^o = 0.0003114888995$

$\omega_8^o = 0.000501383442$

$\omega_7^o = 0.000833137004$

$\omega_6^o = 0.00143892077$ *

$\omega_5^o = 0.00260780157$

$\omega_4^o = 0.00502970452$

$\omega_3^o = 0.01055624269$

$\omega_2^o = 0.02506637347$

$\omega_1^o = 0.0729616142$

$\omega_0^o = 0.3265275274$

---

6 G. N. Watson, "Theory of Bessel Functions," Tables, (1952).

All moments are now slightly readjusted so that the ω_0^o value calculated from Eq. 24 agrees with

$$\omega_0^o = 1 - A\, e^A \left\{ - Ei(-A) \right\}$$

where Ei is an exponential integral.[7]

$$\omega_0^o = 0.326892903$$

Readjusted Values

$$\omega_7^o = 0.0008340692618$$

$$\omega_6^o = 0.001440530883$$

$$\omega_5^o = 0.002610719630$$

$$\omega_4^o = 0.005035332624$$

$$\omega_3^o = 0.01056805484$$

$$\omega_2^o = 0.02509442207$$

$$\omega_1^o = 0.07304325628$$

$$\omega_0^o = 0.326892903$$

---

7 "Tables of Sine, Cosine, and Exponential Integrals," (WPA) Vol. I, (1940).

The equations to be solved simultaneously can now be written down. Even and odd component distributions are to be determined separately, requiring the solution of the two systems

$$\sum_i \alpha_i \beta_i^n = K_n, \quad n = 0, 2, 4, \ldots$$

$$\sum_i \alpha_i \beta_i^n = K_n, \quad n = 1, 3, 5, \ldots$$

where $K_n = J_n/\omega_n^o$.

To the first (even) of these systems one more equation is added which guarantees the known slope change at $x = 0$. To the second (odd) system an equation guaranteeing the known discontinuity is included

$$\sum_i \alpha_i \beta_i^{-2} = A^{-1} \frac{d}{dt} \left(\frac{dT}{dt}\right) \Bigg|_{t = 1}$$

$$\sum_i \alpha_i \beta_i^{-1} = \left(\frac{dT}{dt}\right) \Bigg|_{t = 1}$$

To insure the asymptotic trend, one of the β_i's, say β_2, may be set equal to unity.

The equations may be solved by a method introduced by Spencer.[8] Define

$$D_n = K_n - K_{n-2}$$

---

[8] L. V. Spencer, Phys. Rev. 88, 793 (1952).

$$K_{-1} = \left.\frac{dT}{dt}\right|_{t = 1}$$

$$K_{-2} = A^{-1} \left.\frac{d}{dt}\left(\frac{dT}{dt}\right)\right|_{t = 1}$$

For odd n,

$$b = \frac{D_7D_1 - D_5D_3}{D_5D_1 - D_3^2}$$

$$= 1.124999108$$

$$c = \frac{bD_3 - D_5}{D_1}$$

$$= 0.1904757641$$

$$\beta_o^2 = \frac{b - \sqrt{b^2 - 4c}}{2}$$

$$= 0.207633404$$

$$\beta_1^2 = \frac{b + \sqrt{b^2 - 4c}}{2}$$

$$= 0.917365702$$

$$\alpha_o^* = \frac{D_1\beta_1^2 - D_3}{\sqrt{b^2 - 4c}}$$

$$= 0.202706138$$

$$\alpha_1^* = D_1 - \alpha_o$$

$$= 0.195157850$$

$$\alpha_o = \frac{\alpha_o^* \beta_o}{\beta_o^2 - 1}$$

$$= 0.116570687$$

$$\alpha_1 = \frac{\alpha_1^* \beta_1}{\beta_1^2 - 1}$$

$$= - 2.26202256$$

$$\alpha_2 = K_{-1} - \frac{\alpha_o}{\beta_o} - \frac{\alpha_1}{\beta_1}$$

$$= 2.68136$$

$$\alpha_2 = K_1 - \alpha_o\beta_o - \alpha_1\beta_1$$

$$= 2.68136887$$

For even n,

$$b = \frac{D_6 D_o - D_4 D_2}{D_4 D_o - D_2^2}$$

$$= 1.089084046$$

$$c = \frac{bD_2 - D_4}{D_o}$$

$$= 0.2059259267$$

$$\beta_o^2 = \frac{b - \sqrt{b^2 - 4c}}{2}$$

$$= 0.243543538$$

$$\beta_1^2 = \frac{b + \sqrt{b^2 - 4c}}{2}$$

$$= 0.84540458$$

$$\alpha_o^* = \frac{D_o \beta_1^2 - D_2}{\sqrt{b^2 - 4c}}$$

$$= 0.123682909$$

$$\alpha_1^* = D_o - \alpha_o^*$$

$$= 0.250568832$$

$$\alpha_o = \frac{\alpha_o^* \beta_o^2}{\beta_o^2 - 1}$$

$$= - 0.0398201017$$

$$\alpha_1 = \frac{\alpha_1^* \beta_1^2}{\beta_1^2 - 1}$$

$$= - 1.371660709$$

$$\alpha_2 = K_{-2} - \frac{\alpha_o}{\beta_o^2} - \frac{\alpha_1}{\beta_1^2}$$

$$= 1.765157521$$

$$\alpha_2 = K_o - \alpha_o - \alpha_1$$

$$= 1.765157522$$

$J(x)$ for either n odd or n even is evaluated by the relation

$$J(x) = \sum_i \frac{\alpha_i}{\beta_i} e^{-Ax/(\beta_i - x)}$$

where the numbers α_i and β_i vary as n is odd and even. Then, $\overset{\text{odd}}{J}(x)$ and $\overset{\text{even}}{J}(x)$ combine to give $J(x)$ by

$$J(x) = \frac{\overset{\text{even n}}{J}(|x|) + \operatorname{sgn} x \, \overset{\text{odd n}}{J}(|x|)}{2}$$

x	odd n $J(x)$	even n $J(x)$	$\frac{\overset{\text{even}}{J}(x) + \overset{\text{odd}}{J}(x)}{2}$	$\frac{\overset{\text{even}}{J}(x) - \overset{\text{odd}}{J}(x)}{2}$
0	0.06383	0.19278	0.12831	0.06448
0.02	0.07444	0.19344	0.13394	0.05950
0.04	0.08529	0.19422	0.13978	0.05447
0.06	0.09645	0.19503	0.14574	0.04929
0.08	0.10777	0.19591	0.15184	0.04407
0.10	0.11929	0.19687	0.15808	0.03879
0.15	0.14784	0.19827	0.17306	0.02522
0.20	0.17416	0.20096	0.18756	0.01340
0.25	0.19463	0.20013	0.19738	0.00275
0.30	0.20385	0.19853	0.20119	-------
0.35	0.19781	0.19127	0.19454	
0.40	0.18047	0.17879	0.17963	
0.50	0.13880	0.14367	0.14123	
0.60	0.09113	0.09606	0.09360	
0.70	0.04013	0.04029	0.04021	
0.80	0.00528	0.00406	0.00467	
1.00	-------	-------	-------	

The resultant distribution for 50 kev is shown in Fig. 3. Also, individual distributions were constructed for 75, 100, and 125 kev and are shown in Figs. 4, 5, and 6, respectively.

IV. THEORY OF TRIPLE PLATE IONIZATION CHAMBER

The triple plate ionization chamber is an instrument which is designed to measure the spatial distribution of electron depth dose in an approximation to an infinite medium of aluminum. The general principles used were first suggested by Spencer and Fano.

Consider the spatial distribution of energy loss due to an electron born in an infinite medium with the Figs. 7, 8, 9, and 10, representing a cross-sectional view of such a medium. Assume that the air-filled cavities, A and B, are small enough not to disturb the electron flux appreciably. According to the Bragg-Gray principle, the ionization in the cavities will be proportional to the energy dissipation rate in the medium. In Fig. 7 an electron is born at $x = 0$ and travels in a positive x direction. The ionization in cavity B is proportional to the rate of energy dissipation at this point. An analogous situation takes place in the triple plate ion chamber sketched in Fig. 9. Here, plate number 3 (whose thickness may be varied) represents the positive distance x in Fig. 7. Plates 2 and 4 are greater in thickness than the electron range. In Fig. 9, the ionization current in cavity B is collected with a battery and meter No. 4 is proportional to the rate of energy dissipation. The spatial distribution in the positive x direction may be constructed by varying the position of cavity B in the medium by changing the thickness

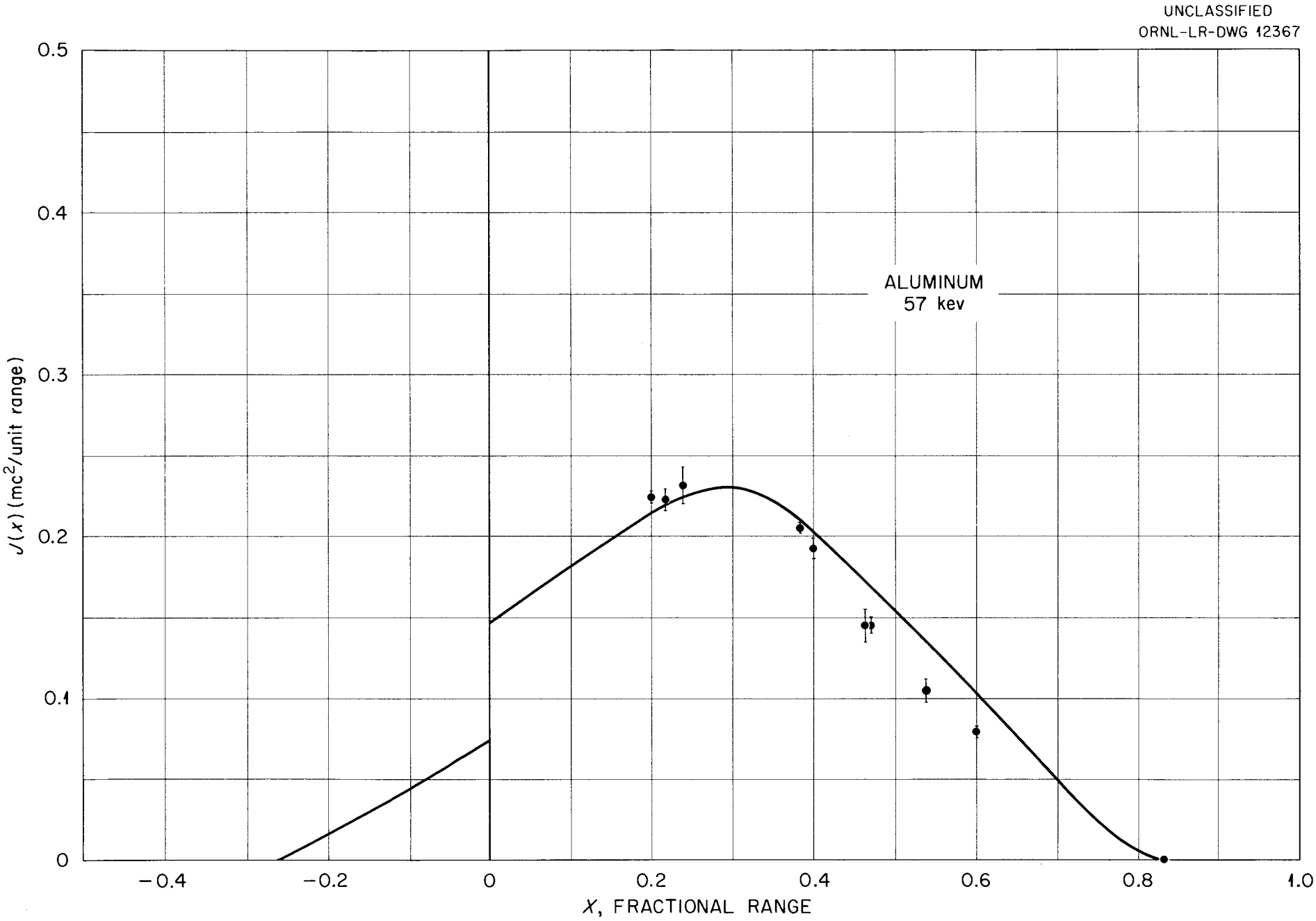

FIG. 3- SPATIAL DISTRIBUTION OF DOSAGE AS A FUNCTION OF PENETRATION DEPTH. POINTS ARE EXPERIMENTAL VALUES AND SOLID LINE IS SPENCER THEORY.

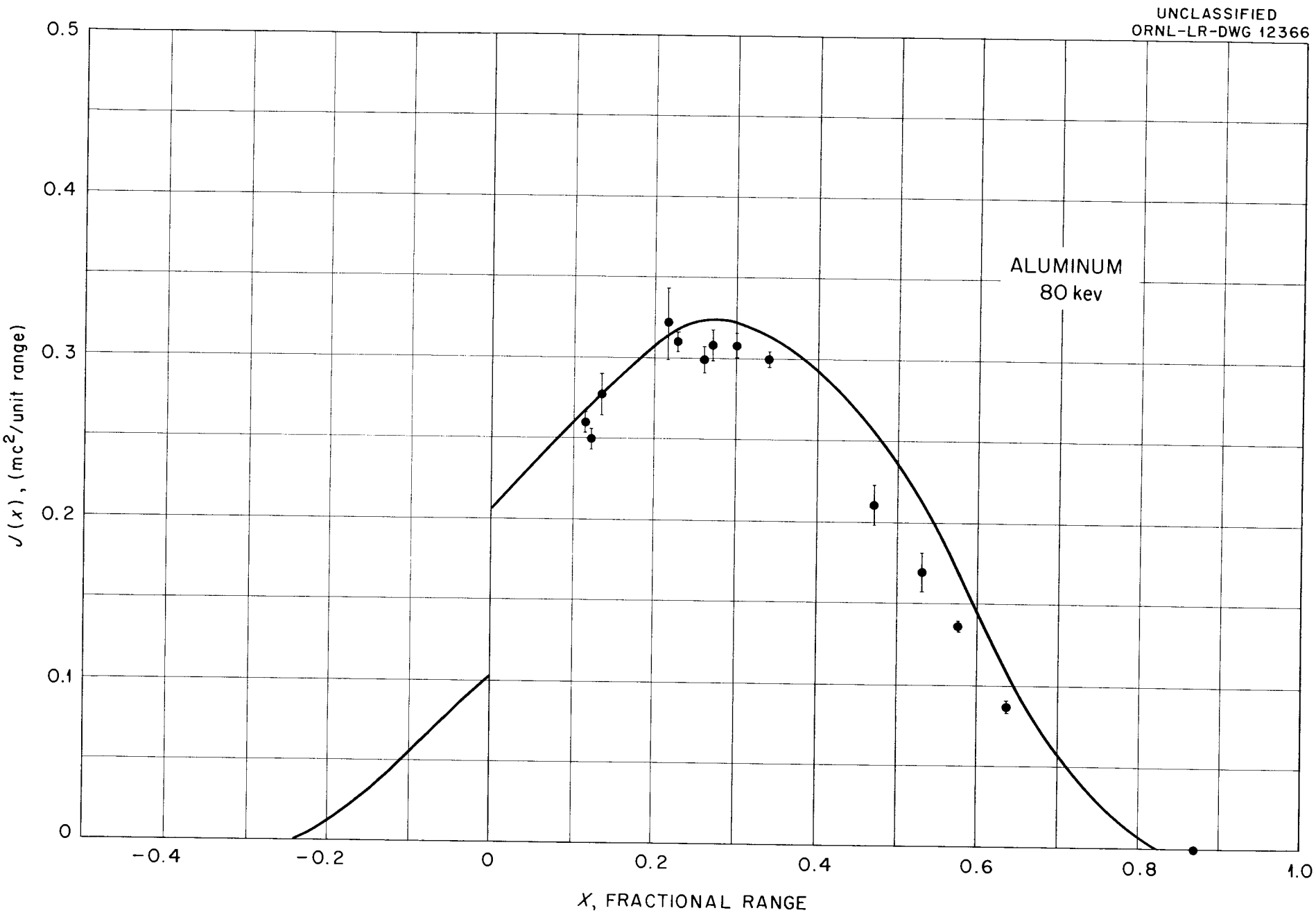

FIG. 4-SPATIAL DISTRIBUTION OF DOSAGE AS A FUNCTION OF PENETRATION DEPTH. POINTS ARE EXPERIMENTAL VALUES AND SOLID LINE IS SPENCER THEORY.

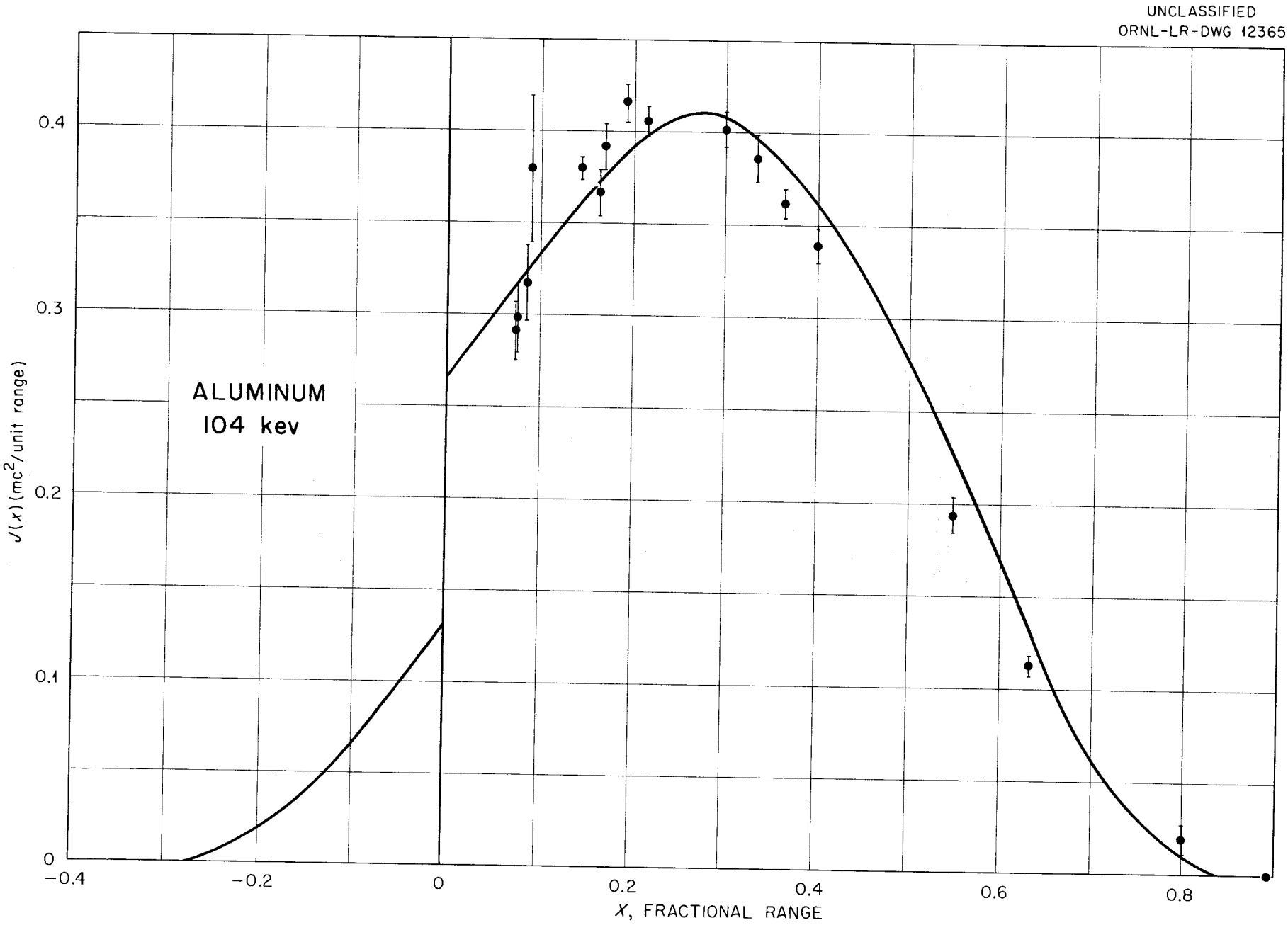

FIG. 5 - SPATIAL DISTRIBUTION OF DOSAGE AS A FUNCTION OF PENETRATION DEPTH. POINTS ARE EXPERIMENTAL VALUES AND SOLID LINE IS SPENCER THEORY.

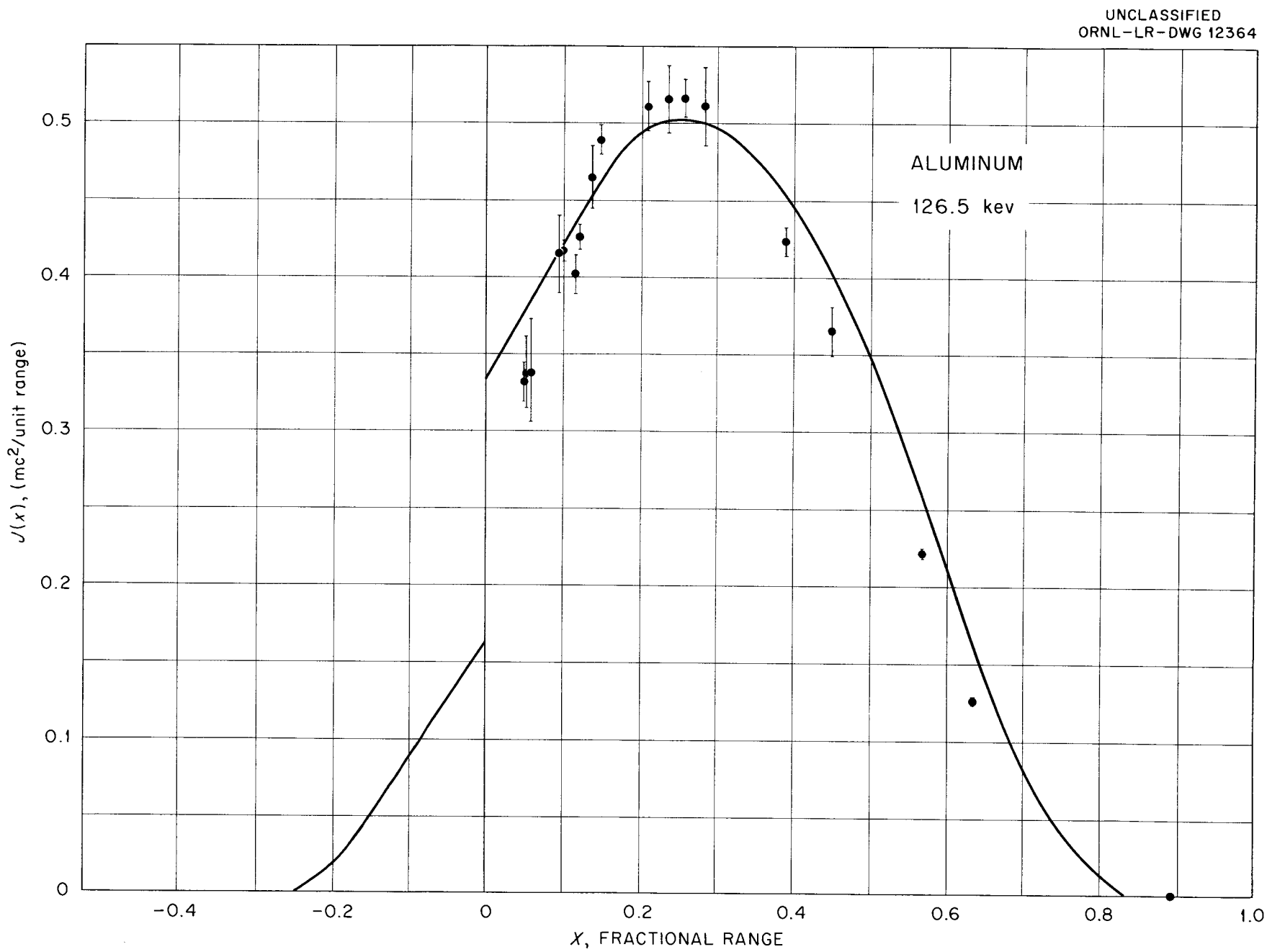

FIG. 6 – SPATIAL DISTRIBUTION OF DOSAGE AS A FUNCTION OF PENETRATION DEPTH. POINTS ARE EXPERIMENTAL VALUES AND SOLID LINE IS SPENCER THEORY.

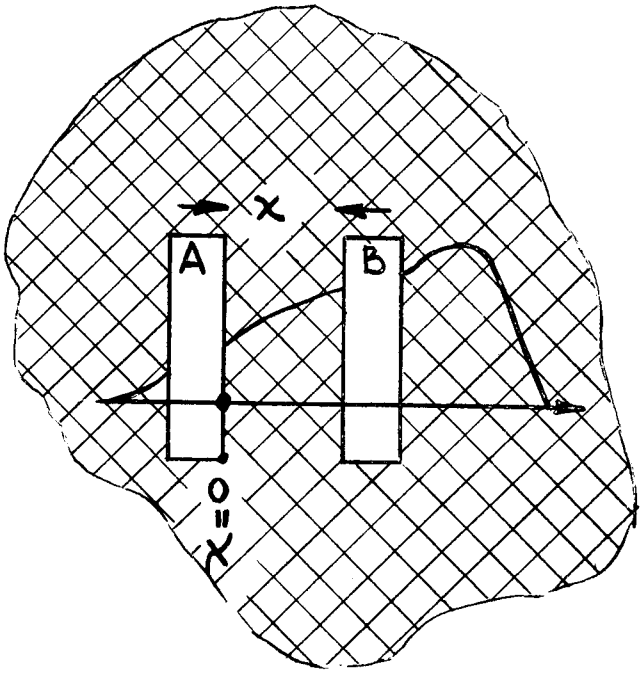

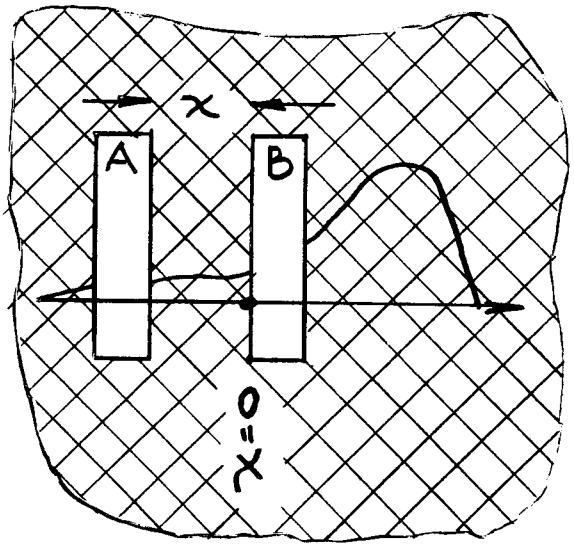

Note shift of origin

Fig. 7
Positive x Distribution

Fig. 8
Negative x Distribution

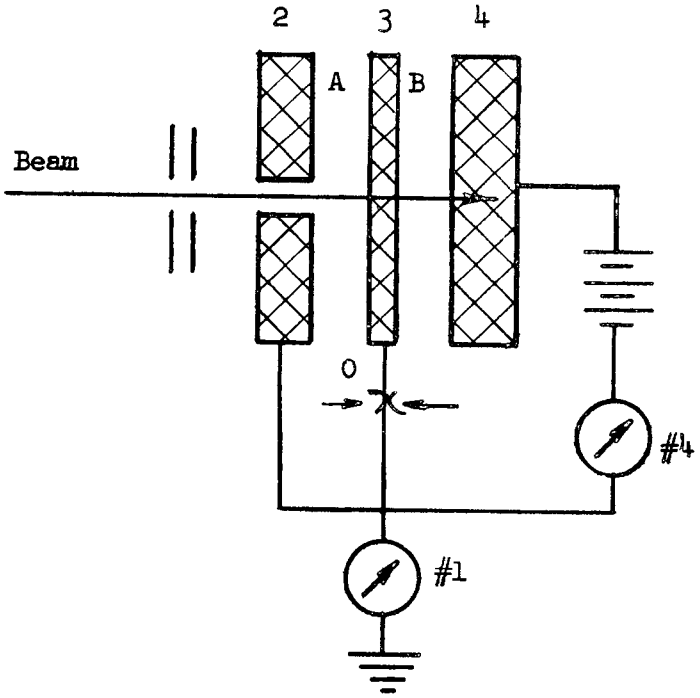

Fig. 9

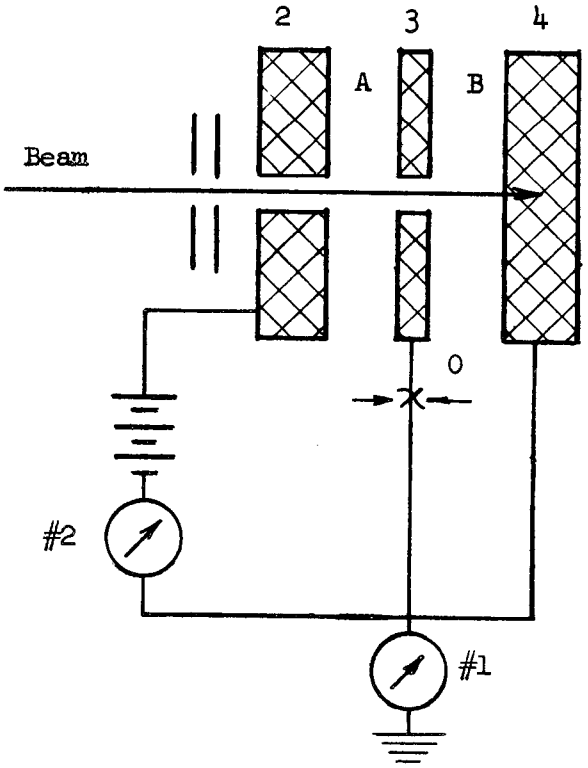

of plate 3.

The situation for measuring the backscattered dose (negative x) is sketched in Figs. 8 and 10. Note that the position of x = 0 has changed and that plate 3 now determines the negative distance x. In this case, the ionization in cavity A is proportional to the back-scattered energy dissipation rate.

Obviously, meter No. 1 (in the circuits sketches in Figs. 9, 10, and 14) will record the total beam current into the chamber. Also, $I_1 = I_2 + I_3 + I_4$ regardless of the direction or magnitude of the ion current. The ratio of ion current to total beam current gives ion pair/electron. However, I_4 consists of a fraction of I_1 plus or minus the ion current. Ion current and I_4 are functions of cavity pressure. Therefore, if the ratio of I_4/I_1 is plotted against pressure, the slope of the line through these points will represent ion pair/electron/unit pressure. When this quantity is substituted in the expression below, a value of J(x) $mc^2/g/cm^2$/electron can be obtained.

$$J(x)\ \frac{mc^2}{el\ -\ g/cm^2} = \left(\frac{I_4}{I_1}\ \frac{i.p.}{el}\right)\left(\frac{34\ ev}{i.p.}\right)\left(\frac{293\ K^o}{273\ K^o}\right)\left(\frac{1}{p\ cm\ Hg}\right)\left(\frac{76\ cm\ Hg}{1}\right)$$

$$\left(\frac{1}{0.001293\ g/cm^3}\right)\left(\frac{1}{d\ cm}\right)\left(\frac{1}{0.511 \times 10^6\ ev/mc^2}\right)$$

d = depth of chamber

Fig. 11 and Fig. 12 show constructional details of the chamber.

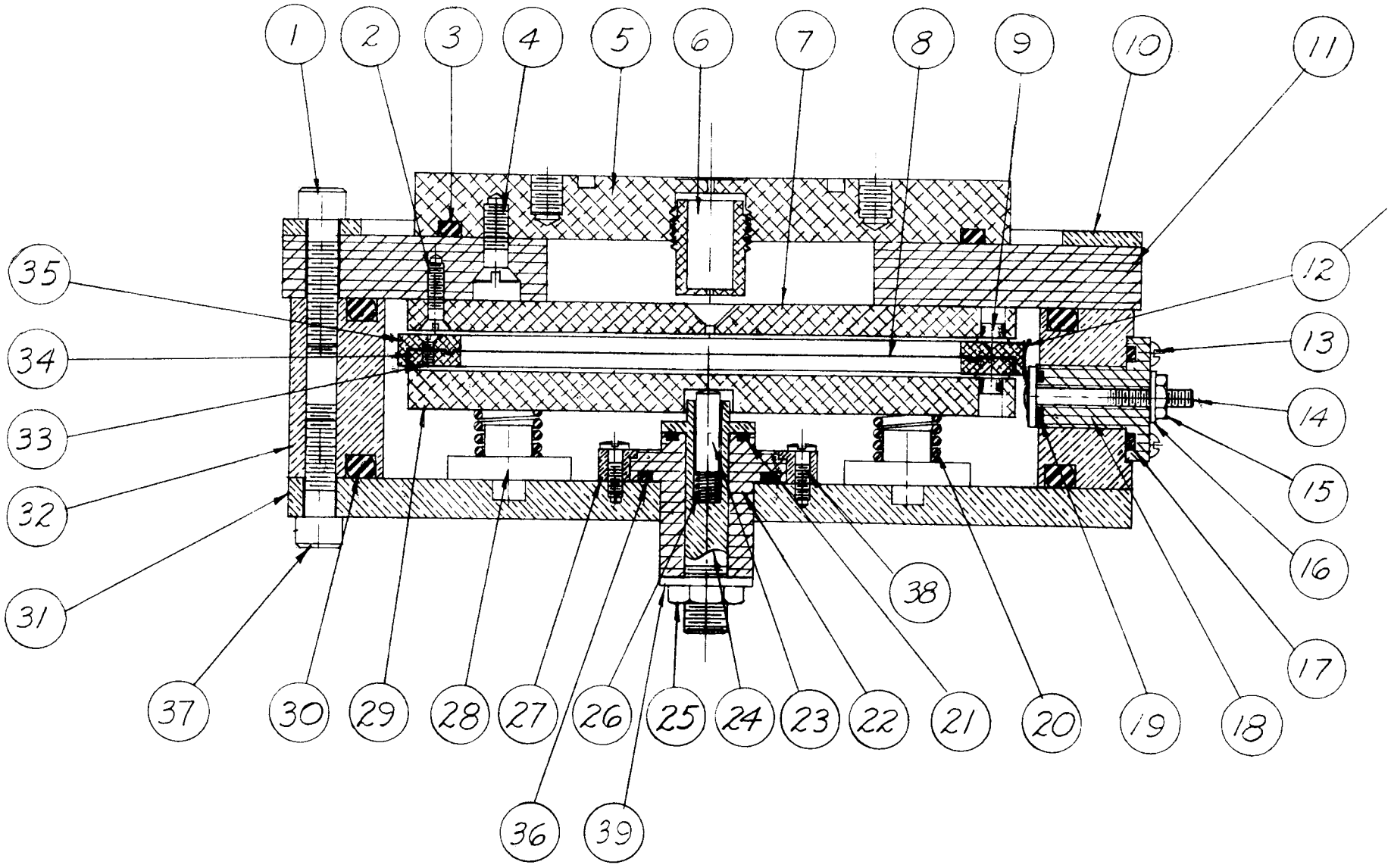

Fig. 11 Cross Sectional View of Triple Plate Ion Chamber

Photo-17169
UNCLASSIFIED

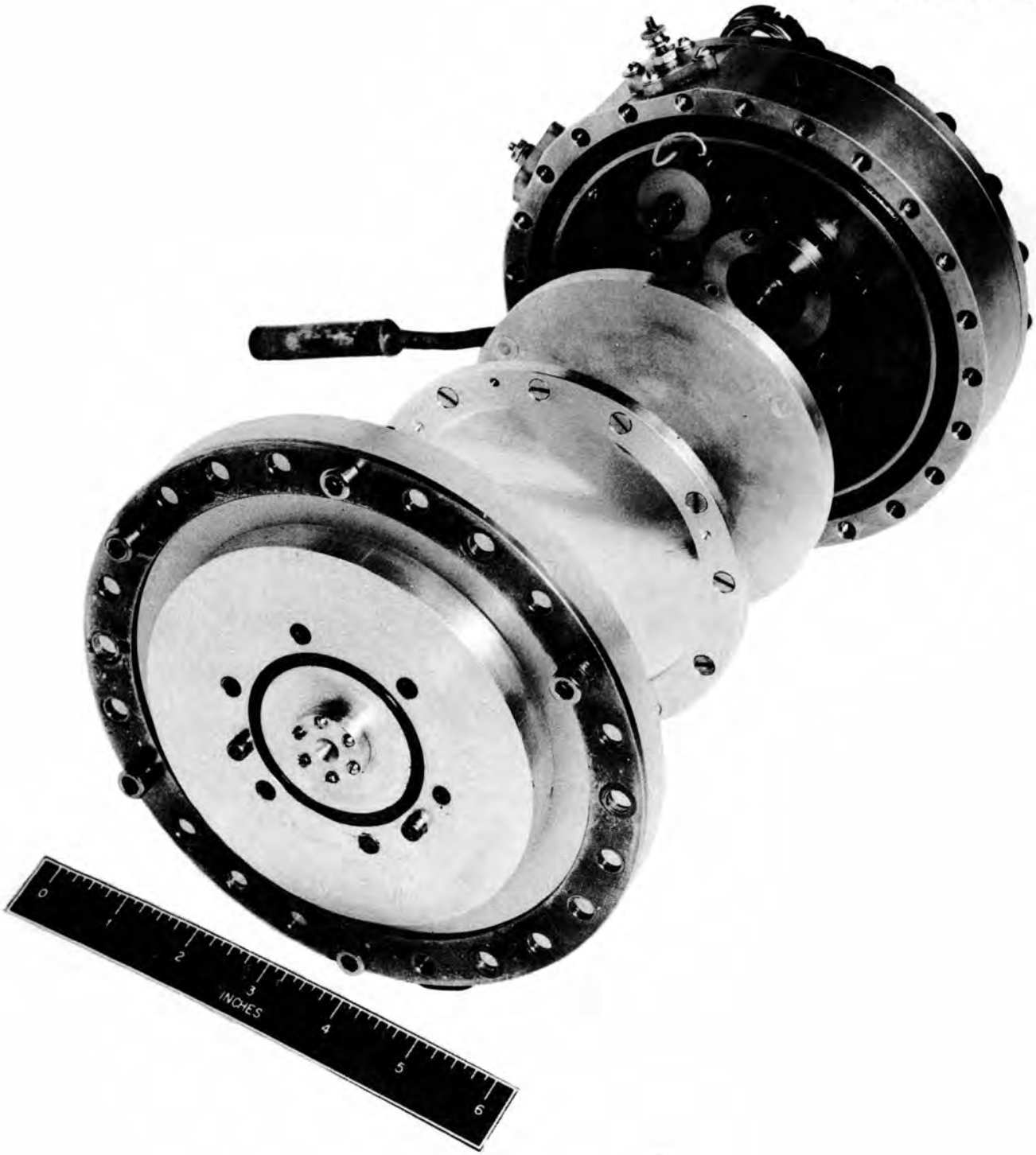

Fig. 12 Photograph of Triple Plate Ion Chamber

Parts List for Ion Chamber Shown in Fig. 11

Part No.

1. Soc. Hd. Cap Scr. (Steel)
2. Flat Hd. Mach Scr. (Steel)
3. "O" Rine # 6227 (Neoprene)
4. Flat Hd. Mach Scr. # 10-24 (24ST-Al)
5. Adapter Plate (24ST-Al)
6. Collimator (24ST-Al)
7. Inside Disc (2S-Al)
8. Aluminum Foil (2S-Al)
9. Insulating Spacer (Fluorothene)
10. Insulator Plate Retainer (Brass)
11. Insulator Plate (Fluorothene)
12. Contact Leaf (Be Cu)
13. Rd. Hd. Mach Scr. (Steel)
14. Terminal Pin (Copper)
15. Hex Nut # 5 (Steel)
16. Flat Washer # 5 (Steel)
17. "O" Ring # 6227-11 (Neoprene)
18. Insulator (Fluorothene)
19. "O" Ring # 6227-5 (Neoprene)
20. Level Spring (Be Cu)
21. "O" Ring # 6227-9 (Neoprene)
22. End Seal Insulator(Fluorothene)
23. Contact Pin (Copper)
24. End Seal Terminal (Copper)
25. Jam Nut (Steel)
26. Contact Spring (Be Cu)
27. End Seal Retainer (Brass)
28. Insulating Ring Guide (Fluorothene)
29. Outside Disc (2S-Al)
30. "O" Ring # 6227-59 (Neoprene)
31. End Plate (Brass)
32. Housing (Brass)
33. Flat Hd. Mach Scr. (Steel)
34. Female Foil Holder (24ST-Al)
35. Male Foil Holder
36. "O" Ring # 6227-17 (Neoprene)
37. Soc. Hd. Cap Scr. (Steel)
38. Rd. Hd. Mach Scr. (Steel)
39. Flat Washer (Steel)

The large lateral dimension of the cavity is necessary to insure essentially complete collection of all ions formed. The linear ion current vs pressure curve shown in Fig. 13 is evidence that the chamber fulfilled this requirement.

The following development by R. H. Ritchie of Oak Ridge National Laboratory demonstrates that the total ionization per incident electron for a small well-defined beam incident on an infinite parallel plate chamber is identical to the total ionization per incident electron for a point chamber with the beam incident over an infinite plane.

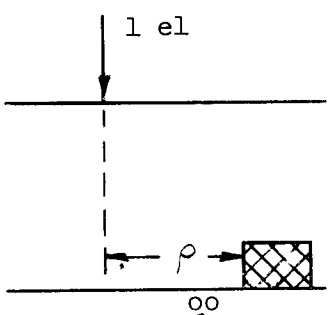

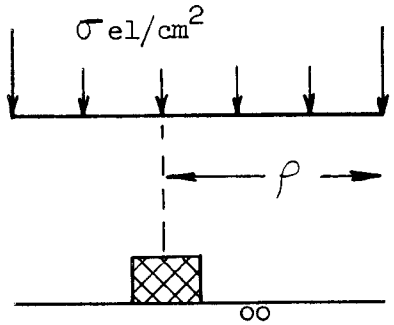

$$I_{Parallel} = \int_0^\infty 2\pi \rho \, d\rho \, F(\rho)$$

$$I_{Point} = \sigma \int_0^\infty 2\pi \rho' \, d\rho' \, F(\rho')$$

But, $f(\rho) = F(\rho')$

Hence, $I_{Point} = \sigma \; I_{Parallel}$

$F(\rho)$ = ionization/cm^2 at a lateral distance from incident electron

σ = number of electrons/cm^2.

I = total ionization.

UNCLASSIFIED
ORNL-LR-DWG. 14868

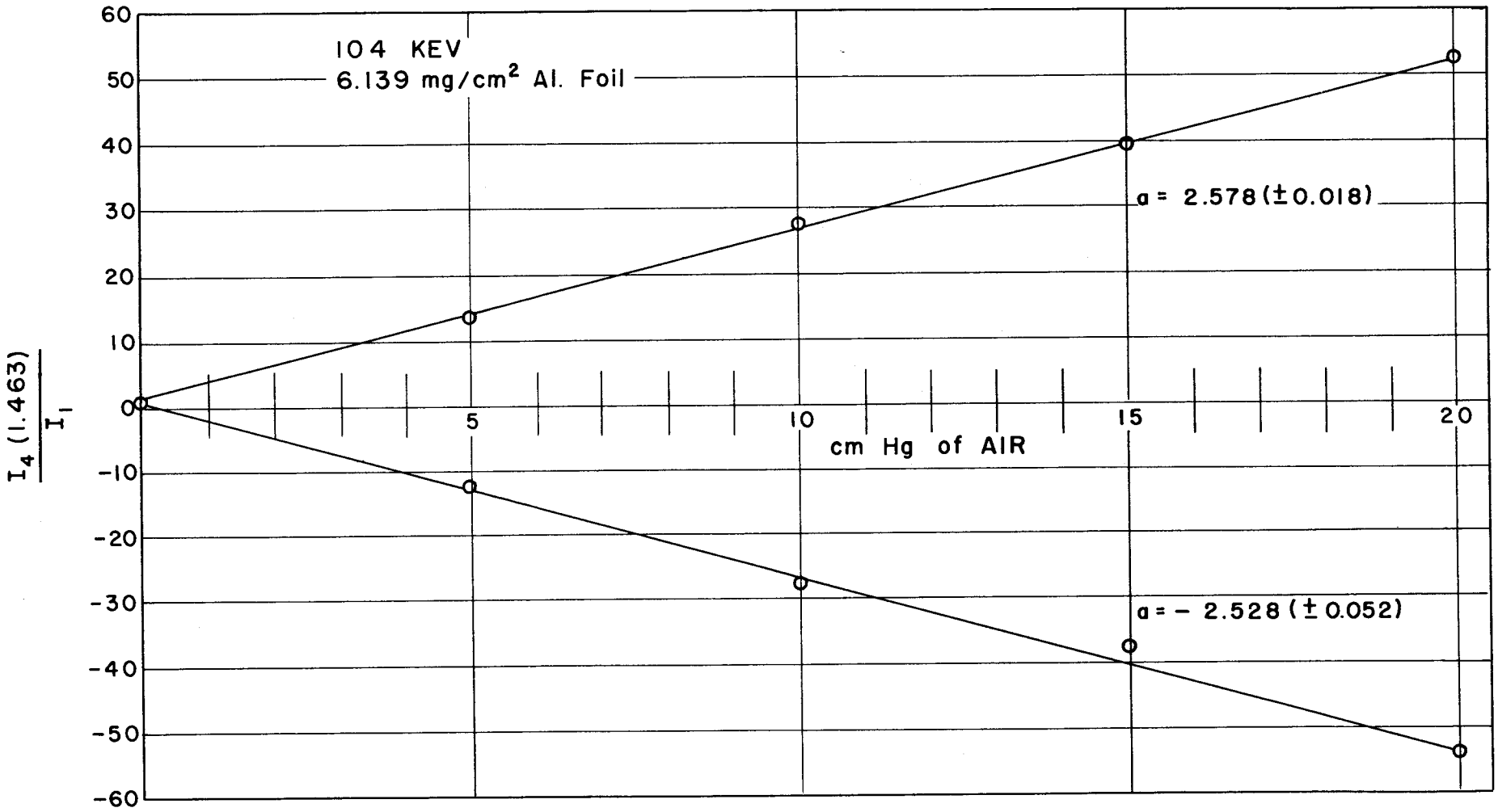

FIG. 13 - TYPICAL PLOT OF INCREMENTAL CURRENT RATIO vs. PRESSURE

V. DESCRIPTION AND DESIGN OF EQUIPMENT

A. Accelerator

A description of the instrument in a slightly modified form has been published by Blackstock, Birkhoff, and Slater.[9] The instrument consists of an electron gun, an accelerating tube, and a tube for either accelerating or decelerating. The accelerating tubes are typical of those used in Cockroft-Walton machines as seen in Fig. 14 and Fig. 15. Each consists of alternate ceramic insulators and accelerating electrodes sealed vacuum tight with vinyl cement. The potentials of the electrodes are established by six fifty megohm IRC voltage dividing resistors in series across the accelerator and six across the decelerator which was grounded in this experiment.

The electron gun used was the gun structure from a General Electric 5 BPI cathode ray tube. The guns were obtained on special order without the screen and cut off at the end of the glass neck. The activation schedule given by the company was followed and gave satisfactory results.

B. Triple Plate Ionization Chamber

The design of the triple plate chamber incorporated available parts from a parallel plate chamber in use at the time. The basic considerations in the chamber design were: 1. Ease of assembly since frequent changing of foils and windows made it necessary for the chamber

---

[9] A. L. Blackstock, R. D. Birkhoff, and M. Slater, Rev. Sci. Instr. 26, 274 (1955).

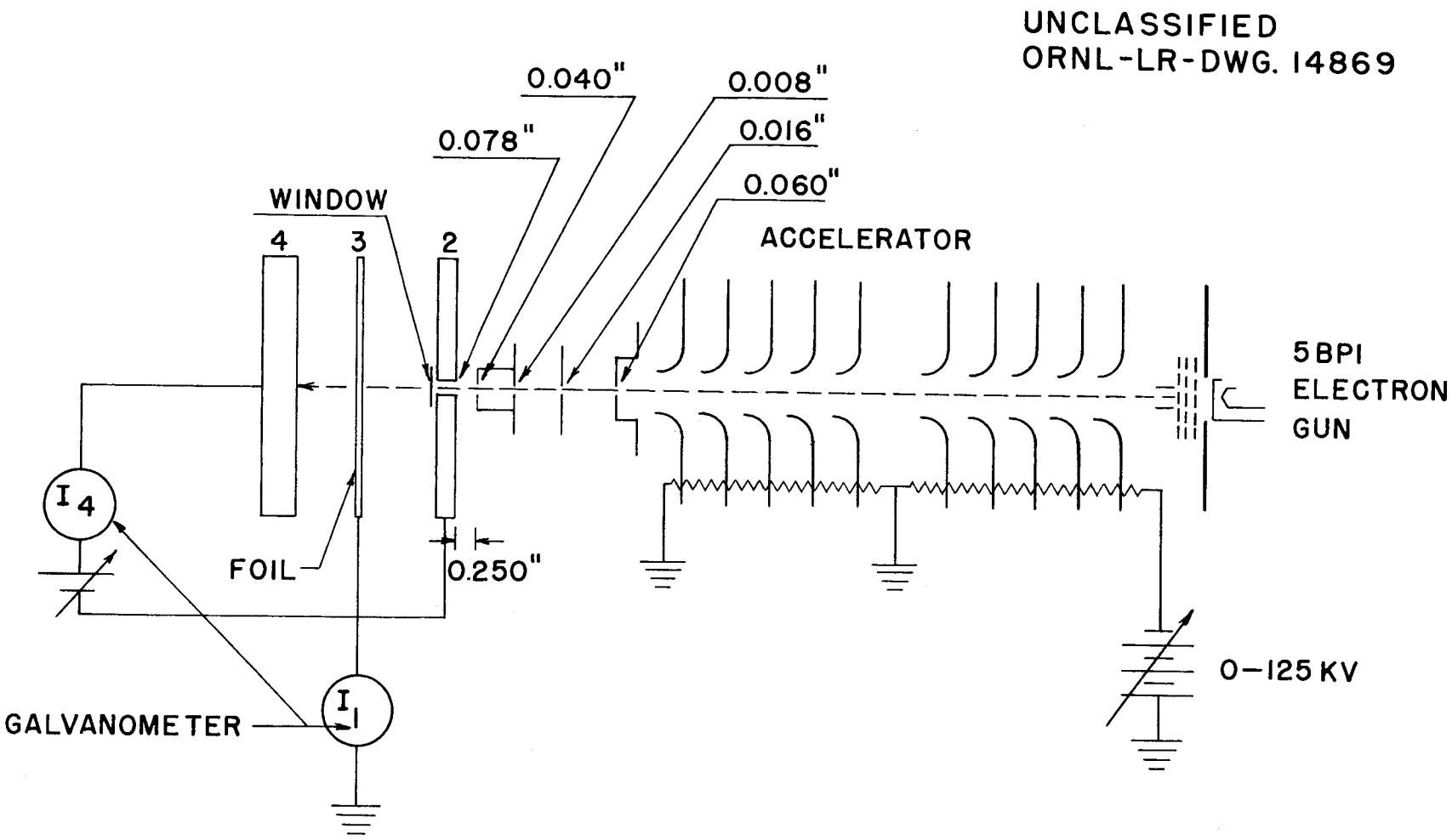

FIG. 14

SCHEMATIC DIAGRAM OF APPARATUS

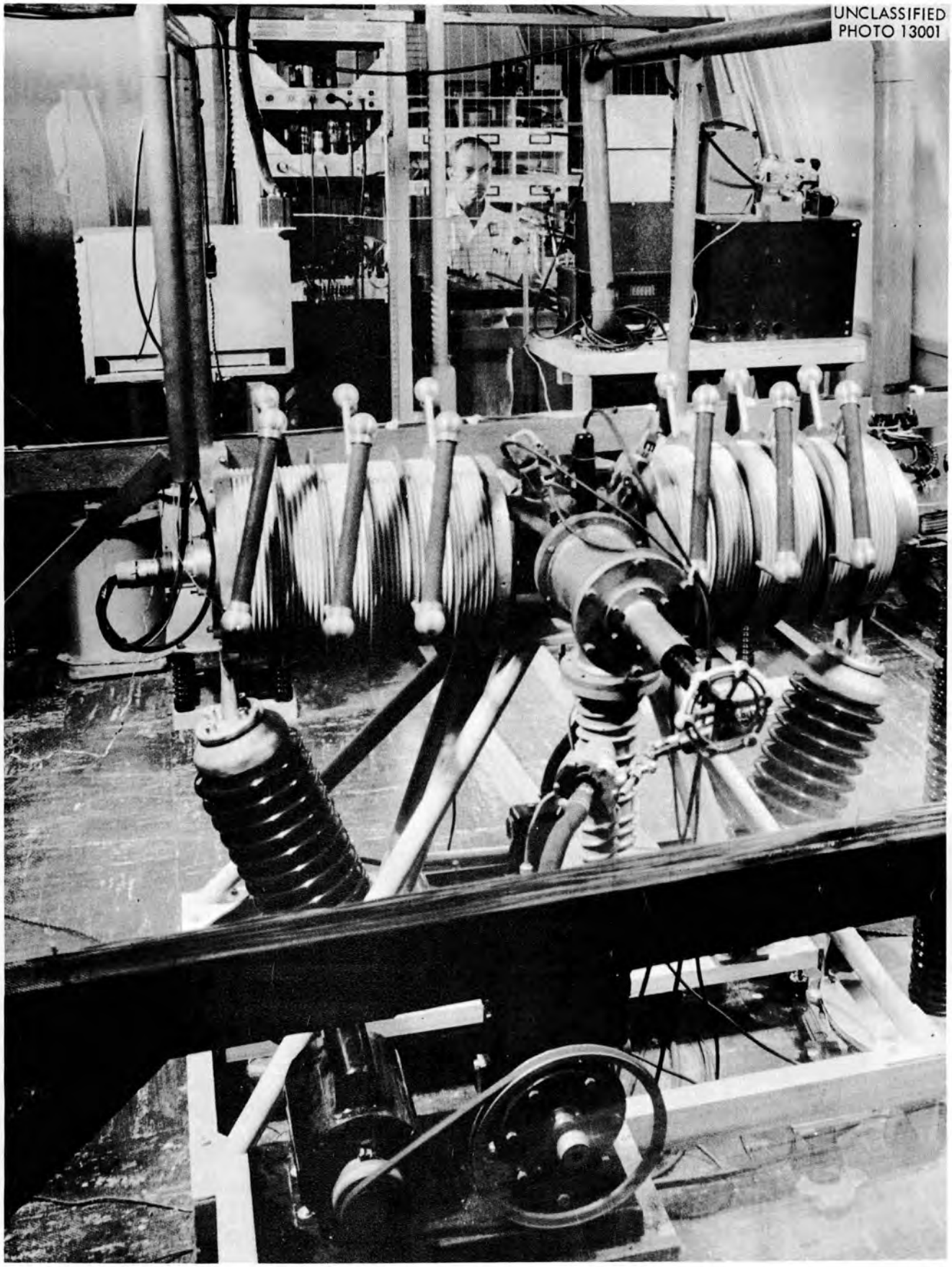

Fig. 15 Photograph of Apparatus

to be taken apart and reassembled readily.

2. Good insulation of ion collector plate which implies that the plate be insulated with a resistance no less than 10^{12} ohms in order that leakage current be no greater than 1%.

3. Narrow collimation of the beam at the entrance aperture (taking into consideration accelerator beam current, galvanometer sensitivity, chamber geometry, and alignment problems) in order that the aperture could be made small so as to subtend a small solid angle for backscattering out of the chamber.

4. Tightly stretched foils since the foils formed one plate of the ion chamber, and hence it was necessary that the foils be plane within 0.005 in. to give a uniform electric field for ion collection.

5. Maintenance of spacing between foil and backplate. Since this spacing was only 0.156 in., it was necessary to design a means for replacing foils without disturbing the chamber depth more than 0.002 in. The above considerations were embodied in the design shown in Fig. 11 and Fig. 12.

It should be noted that the apparatus will have to be modified before the method for measuring negative x discussed on Page 42 will be practical.

One of the principal problems encountered was the collection of part of the incident beam on the front plate before the beam entered the chamber. A collecting chamber replaced the backplate (to reduce solid angle of backscattered electrons) when experiments were performed to determine the minimum aperture possible in order that no incident

beam current would be collected on the front plate. At first, the electrons backscattered from the collecting chamber to the front plate confused the results. However, the back surface of the front plate was covered with a sandwich of insulator and foil to avoid collection of backscattered electrons on the front plate. Collimation and aperture size were considered satisfactory when no current was recorded on the front plate with no window over the aperture.

The original plan for introducing the beam from the accelerator into the ion chamber was to use an aluminum window in front of the last collimators thin enough not to affect seriously the energy or angular distributions of the electrons incident on the foil. However, a window thin enough to satisfy these conditions broke in a few minutes under a recordable beam (approximately 10^{-8} amp) and with a few cm Hg of air in the ion chamber. The next most attractive alternative seemed to be the use of differential pumping. "Cut and try" methods yielded a pumping system satisfactory as far as pressure in the accelerator tank was concerned, but increased positive ion bombardment gave a rapid deterioration of the gun and introduced critical adjustment of electron gun potentials. Also, the reduced chamber extrapolation pressure was difficult to measure under dynamic conditions. These factors forced the abandonment of this procedure. For the taking of data, a thin aluminum coated mylar window (approximately 1 mg/cm^2) was cemented to the inside of the front plate. Electrical contact was made with aquadag. In this case, the window thickness was added to the foil thickness to give the total penetration depth. The backscattering and secondary electrons lost (i.e., not read as part of I_1) were considered

negligible because of the very thin window and the small angle subtended by the aperture from the foil and backplate. All of the incident electrons, including backscattered and secondaries must be collected if an absolute measurement is to be made. Otherwise, the dose/electron will be in error. Because of the inclusion of the thin foil for the window, a new geometry will have to be devised for measuring the negative distribution. This measurement is complicated by the incident beam ionization since we wish to measure the ionization only from electrons that are backscattered from the backplate and pass through the foil. This may be accomplished by subtracting the contribution of the beam (measured with a punctured foil thicker than the range of the incident electrons) from the usual extrapolation measurement.

C. Differential Pumping

In order to dispense with a window between the ion chamber and the accelerator, a system of differential pumping was developed. Several chambers with beam apertures as small as possible were constructed and combined with the fastest possible pumping on each chamber using available equipment. Satisfactory results were obtained with a Kinney VSD 556 (rated pumping speed of 8 cubic feet per second at 1000 microns) on the "Tee" chamber shown in Fig. 16, a DPI booster VKB-8 Oil Ejector Pump (7 ℓ/s at 75 microns) backed by a CENCO-Megavac ($\frac{1}{2}$ ℓ/s at 100 microns) on the "gate" valve. The accelerator itself used a DPI VMF 260R Oil Diffusion Pump (20 ℓ/s) (in combination with a liquid air jacket) backed by a Welch Duo-Seal.

The sizes of the beam aperture holes for the accelerator, "Tee" chamber, and ion chamber are respectively 0.060, 0.016, and 0.008 inches in diameter.

The design of the "Tee" chamber was dictated by the bolt circles in use, available fittings, and ease of construction rather than any theoretical requirements and is shown in Fig. 16. The beam collimator is detachable and is sealed with a small "O" ring.

The operating pressure in the accelerator tank was kept below 10^{-4} mm Hg to avoid power supply overload and arcing inside the accelerator. A maximum of six cm Hg of air pressure could be allowed in the ion chamber without exceeding the operating pressure in the accelerator. To improve the accuracy of the pressure readings, the mercury manometer was replaced with one using butyl phthalate, expanding the scale by a factor of approximately thirteen.

With air in the ion chamber, the high filament current necessary to maintain an adequate beam shortened the gun life to a few days. Apparently the difficulty was caused by positive ion bombardment of the cathode. A twenty mesh screen was inserted between the accelerating tube and the grounded tube in order to give an essentially field-free region to avoid accelerating positive ions toward the electron gun. The gun emission would recover if the air were pumped from the ion chamber. Critical adjustment of the gun potentials and degaussing fields were required to maintain the beam. In spite of these difficulties, data were taken on several foils. Unfortunately, the data were erratic and useless for a quantitative measurement.

The effect of the air gradient on electron scattering and energy

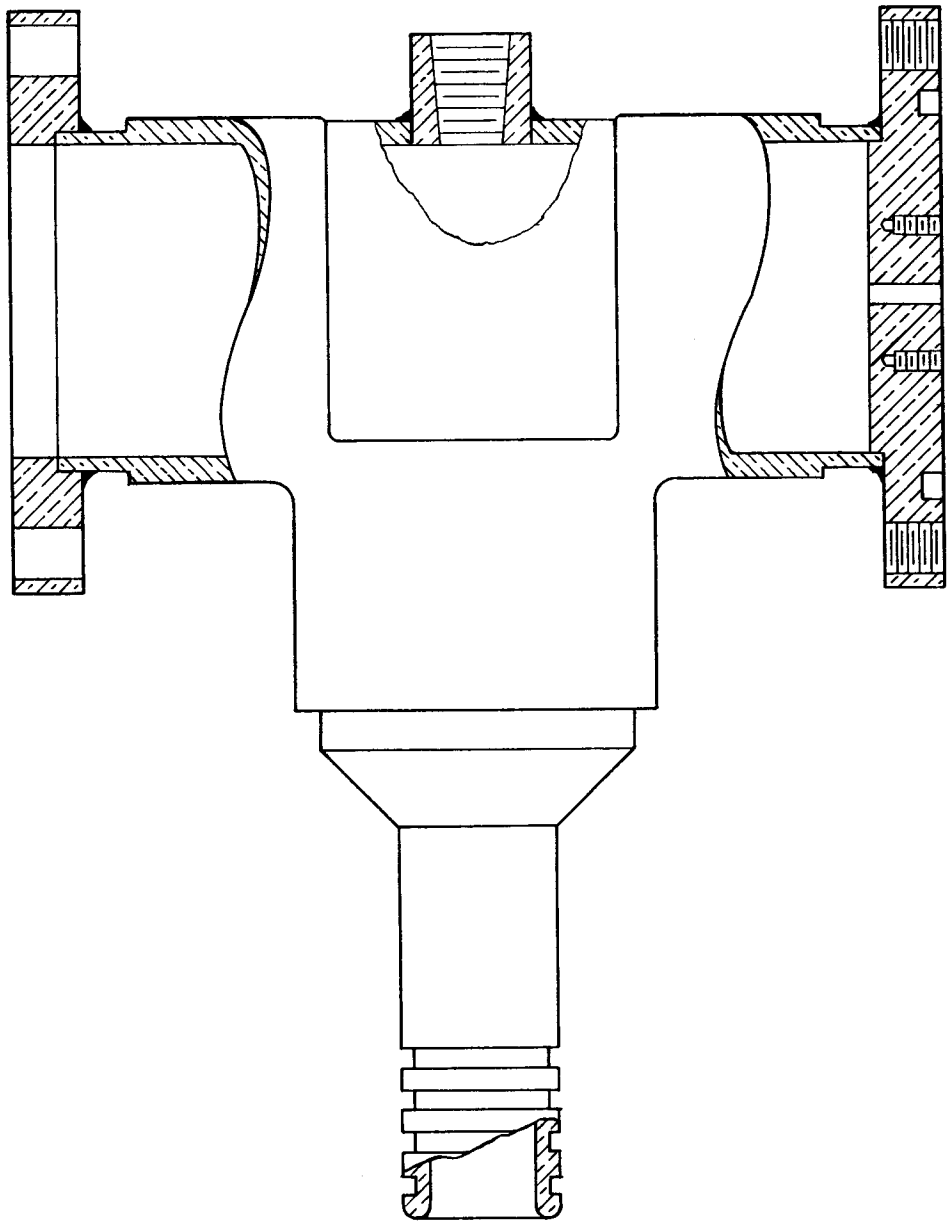

FIG. 16

CROSS SECTIONAL VIEW OF "TEE" CHAMBER

UNCLASSIFIED
ORNL-LR-DWG. 14870

loss was also difficult to evaluate. For these reasons, the system of differential pumping was abandoned.

However, the equipment designed for the system was kept in operation as a safety device for the gun. Experience has shown that a "slug" of air from the chamber when the filament is on would greatly shorten the life of the gun or ruin it entirely and seriously overload the high voltage supply. Subsequent broken windows justified the above precaution.

D. Beam Positioning

The extremely small holes required for differential pumping made it difficult to get a beam into the ion chamber. Investigation revealed "play" in the bolt circles and the components did not line up perpendicular to the axis of the accelerator. All the faces of the "Tee" and the gate valve were remilled. The components were assembled on a lathe and aligned optically. Then the ion chamber and "Tee" were "pinned" with a dowel fixed in the ion chamber which fitted snugly into a hole in the "Tee". However, the optical alignment was not sufficient to assure a beam because the gun was not necessarily on this optical axis. Additional adjustment was provided by construction of a "positioner" that permitted movement in any direction in the vertical plane with the beam on and the system under high vacuum. Details are shown in Fig. 17. The position of the beam at the entrance to the ion chamber was determined by introducing a plexiglass disc on which concentric circles were machined and which was covered with a fluorescent powder. In general, each new gun required realignment of the system.

UNCLASSIFIED
ORNL-LR-DWG. 14871

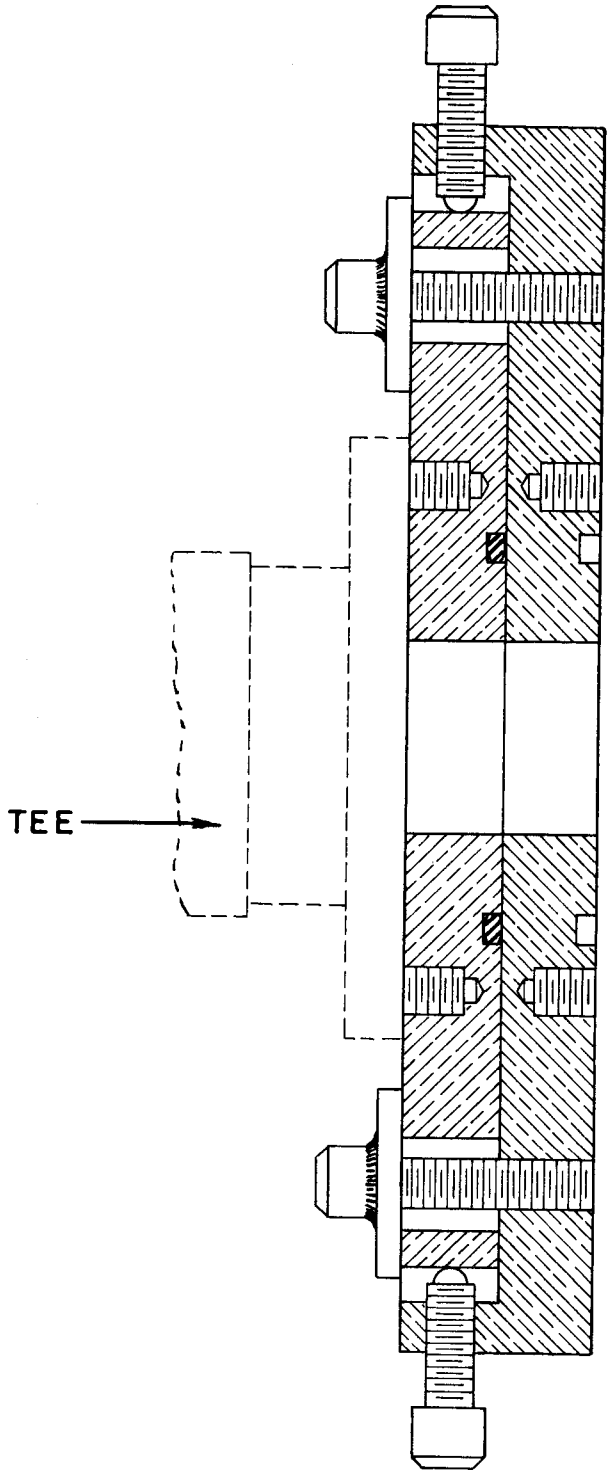

FIG. 17

CROSS SECTIONAL VIEW OF "POSITIONER"

E. Auxiliary Equipment

The source of electrons was an electron gun from a GE 5 BPI employing both electrostatic focussing and deflection. The tubes were shipped unactivated and minus the screen.

The pumping system is described on Page 53 . The pressure was measured with a Consolidated Vacuum Corporation VG-1A ionization gauge. A National Research Corporation Model 501 thermocouple gauge was used to indicate pressures above the range of the ionization gauge. A pressure interlock in the thermocouple gauge control circuit cut off the diffusion pump if the pressure went too high. A valve between the diffusion pump and the rest of the system permitted the system to be brought to atmospheric pressure without allowing the diffusion pump to cool.

The power supply for the electron gun shown in Fig. 18 was designed and built by J. L. Blankenship of the Instrument Division of Oak Ridge National Laboratory. Dual potentiometers permitted the potentials of each member of the two pairs of deflection plates to be varied above and below the second anode potential. Meters were installed so that the voltages of and currents to all gun elements could be monitored. The beam is aimed by varying the potentials of the deflecting plates and focussing electrodes of the gun in combination with adjustment of the horizontal and vertical magnetic degaussing fields.

The high voltage was supplied by a Westinghouse 250 kv x-ray power supply. The supply was center grounded to give maximum flexibility to the accelerator's operation. An oil immersed switch permitted either the accelerator or the x-ray machine to be operated from the same power

UNCLASSIFIED
ORNL-LR-Dwg. 7229

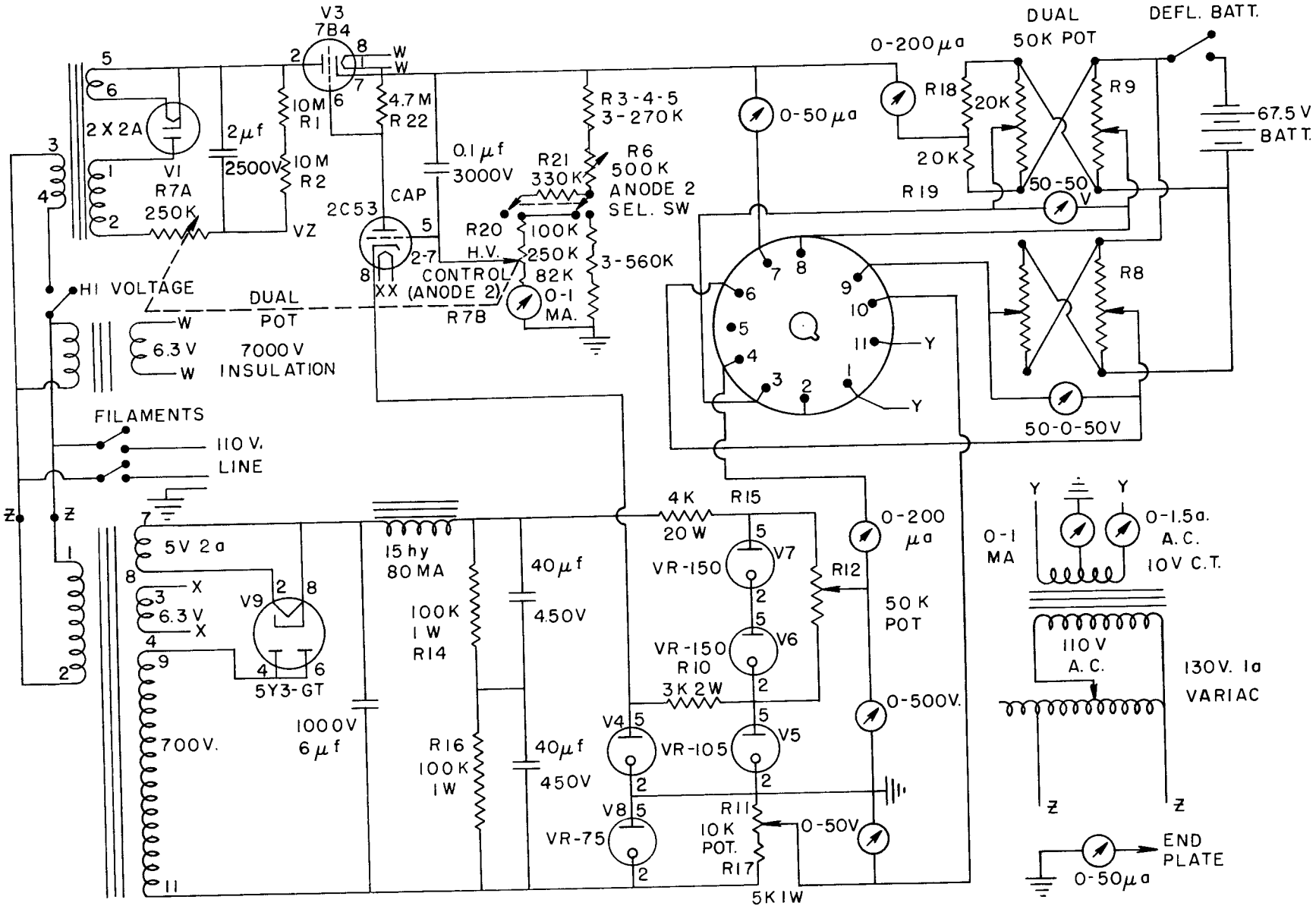

Fig. 18 ELECTRON GUN POWER SUPPLY

supply. Separate controls, designed by Drs. H. Hubbell and M. Slater, permitted the high voltage supply to be operated from the accelerator control panel.

In operation the electron gun and its power supply were at high negative potential. This permitted the ion chamber and its metering circuit to be at ground potential. All equipment at high voltage was enclosed by a screen wire cage. Insulating rods attached to the equipment at high voltage permit the power supply to be operated from outside the cage. The thermocouple and ionization gauge controls, the power supply for the neutralizing coils and the accelerator high voltage controls are mounted in a relay rack which is located at a gap in the cage. Safety interlocks were installed to protect operating personnel. Fig. 15 is a photograph showing the cage, the accelerator and the backs of the control panel and the auxiliary equipment.

The simple metering circuit is diagramed in Fig. 7. A small control box which was constructed to give flexible switching of galvanometer and power supply was abandoned because of the extreme difficulty encountered with high resistance leaks of the order of 10^{10} ohms between switch terminals and connector leads. The leakage was kept within one mm deflection by mounting the control box (containing only the battery power supply) on teflon legs and suspending the wiring from component to component.

The galvanometers used were Rubicon wall (# 2430-D, sens. 0.000678 μa/mm, period 5.7 sec) and a L & N box (# 3515, sens. 0.00046 μa/mm, period 3.2 sec.). Aryton shunts were used on each galvanometer. Meters were overdamped to integrate currents so that the adverse effects of

beam variations would be minimized. The L & N proved to be 1.463 times as sensitive as the Rubicon wall galvanometer.

The assembled system consisting of ion chamber, "Tee", "positioner", and gate valve is shown in Fig. 19.

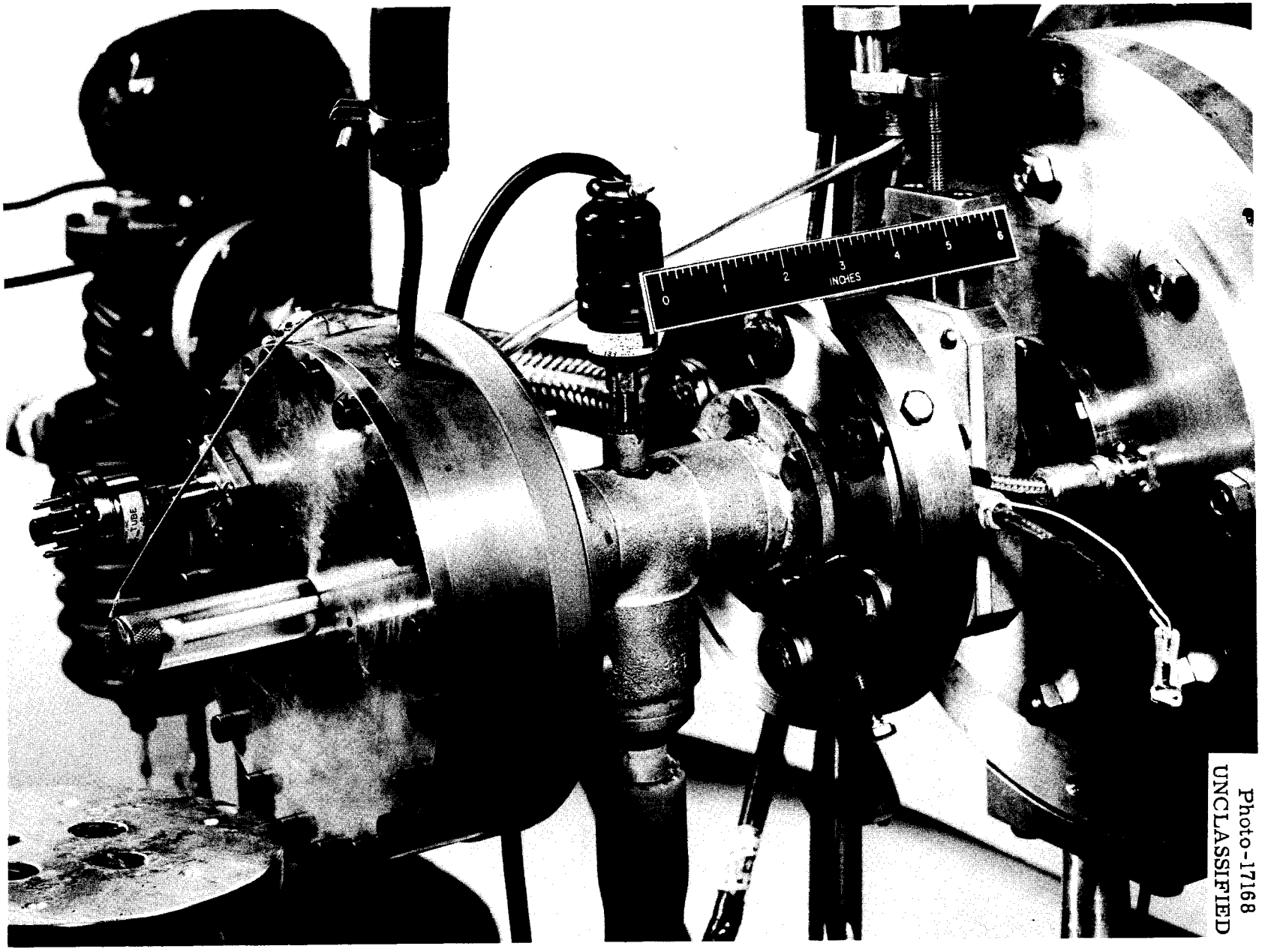

Photo-17168
UNCLASSIFIED

Fig. 19 Photograph of Assembled Apparatus (17168)

VI. TREATMENT OF DATA

A. Sample Calculation

The ratio of I_4 to I_1 was plotted against ion chamber voltage for pressures of 150 microns, 5 cm, 10 cm, 15 cm, and 20 cm Hg as shown in Fig. 20. The chamber depth was maintained constant throughout the experiment. A collection potential was chosen for each pressure and ten readings each of I_4 and I_1 were taken at these potentials for each foil at each incident energy at each pressure and at both positive and negative collection potentials.

I_4 was divided by I_1 and these ten ratios were averaged and plotted vs pressure in cm of Hg. A typical graph is shown in Fig. 13. The slope of the best straight line drawn through these points was substituted into the equation on Page 42 to give J(x) $mc^2/el/g/cm^2$.

It was difficult to average the points and determine the slope visually. For this reason, and for consistency, the slope was determined by a least squares analysis according to the formula[10]

$$a = \frac{\sum x_i y_i - 1/n \sum x_i \sum y_i}{\sum x_i^2 - 1/n \left(\sum x_i\right)}$$

where the x_i's represent the various pressures, the y_i's indicate the corresponding current ratios and n is the number of points determining the slope in each case. Since the data were always taken at the same

---

10 Y. Beers, THEORY OF ERROR, Cambridge: Addison-Wesley, 1953.

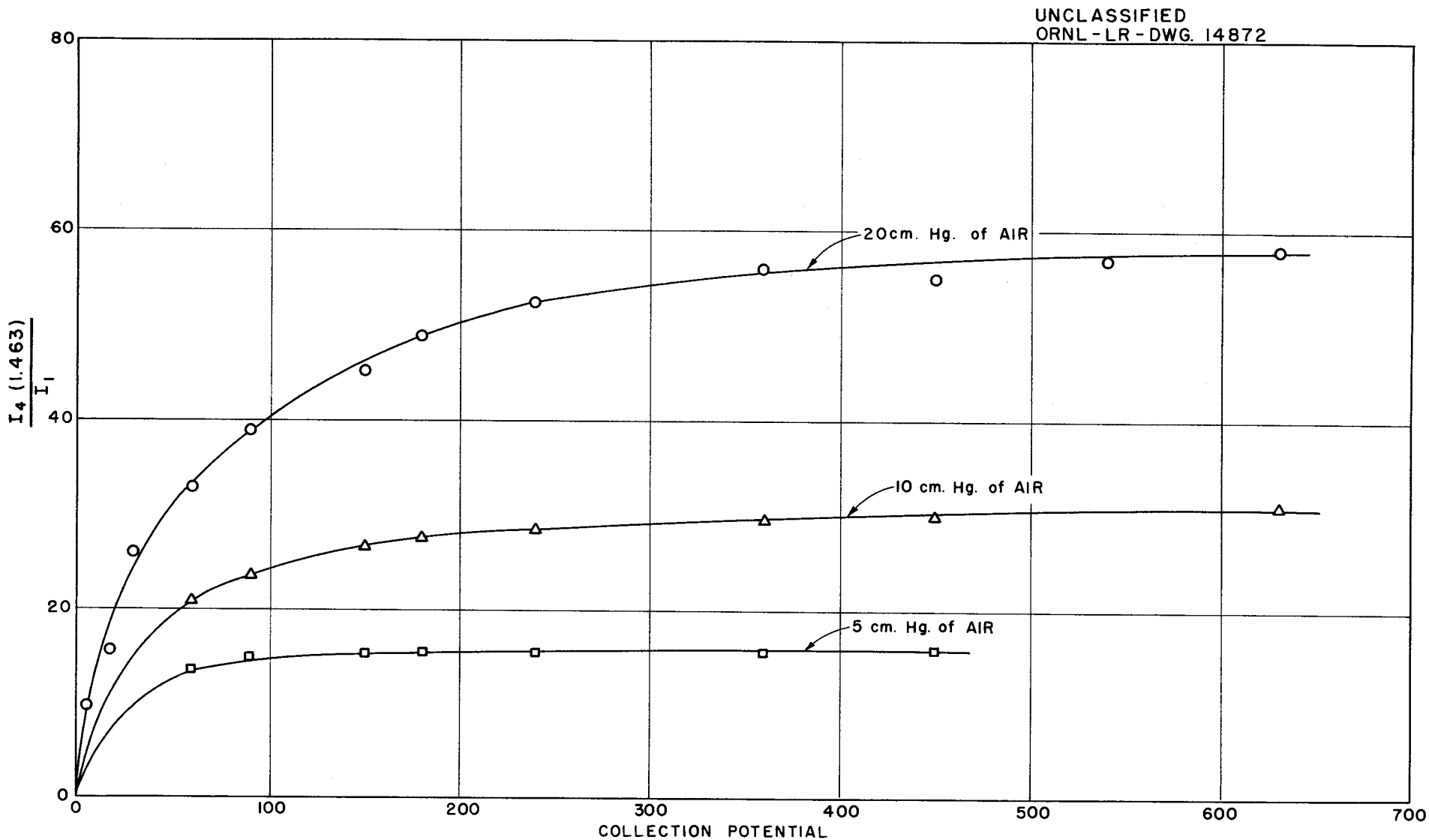

FIG. 20- IONIZATION CHAMBER PLATEAU

five pressures, the equation reduced to

$$a = \frac{\sum x_i y_i - 10 \sum y_i}{250}$$

A typical calculation is given below.

Incident energy - - 104 kev

Foil thickness - - 6.139 mg/cm^2

Positive collection

x_i	y_i	$x_i y_i$
0	0.9428	0
5	13.72	68.6
10	27.52	275.2
15	39.34	590.1
20	52.58	1051.6
	y_i	$x_i y_i$
	134.1028	1985.5

$$a = \frac{644.472}{250} = 2.578$$

Negative collection

x_i	y_i	$x_i y_i$
0	-0.539	0
5	12.62	63.10
10	27.40	274.0
15	37.14	557.1
20	50.39	1007.8
	y_i	$x_i y_i$
	127.011	1902.0

$$a = \frac{631.89}{250} = 2.528$$

average, $\bar{a}$ = 2.553 i.p./el/cm Hg.

$\bar{a}$ is divided by 1.463 to correct for differences in the sensitivities of the galvanometers.

If $W = 34.0$ ev/i.p.

$t = 0.156$ in.,

$$J(x)\ mc^2/el/g/cm^2 = 10.52 \left(\frac{I_4}{I_1} \frac{i.p.}{el\text{-}cm\ Hg} \right)$$

This quantity is converted to $J(x)$ mc^2/unit range by multiplying by the residual range, r_o, of the incident electron. The abscissa $x = z/r_o$, is determined by dividing the thickness of the foil in g/cm^2 by the residual range, r_o, of the incident electron. Note that the foil thickness includes the thickness of the window (0.994 mg/cm^2). In all cases the window was assumed to be entirely of Al although it was a sandwich of Al and mylar. Because the mylar differs only slightly from Al in stopping power and scattering properties and because it was thin compared to the range of the incident electrons, this approximation introduced little error.

The data are presented in Figs. 3, 4, 5, and 6.

B. Estimation of Error

The Spencer theory of the spatial distribution of ionization in a medium involves the extrapolation of a few calculated low-order moments to infinite order. Spencer uses a Wick-type asymptotic calculation to demonstrate that high-order moments need not be calculated if lower order moments can be shown to have the correct asymptotic behavior.

An estimate of error is difficult to make because function fitting techniques have no accompanying test of accuracy comparable with the convergence criteria for polynomial approximations. However, fitting even and odd distributions separately gives an estimate of the accuracy

of the approximation. Since the two component distributions become the same asymptotically, differences which appear in the separate constructions must reflect the error.

Spencer neglects range straggling and assumes that all secondaries are absorbed at the point of origin. The theoretical distributions should be altered little by these approximations.

The accuracy of the construction is dependent on the Mott single scattering theory and the validity of the Bethe stopping power formula, both at low energies. The discrepancy between Mott theory and experiment in this range has apparently been resolved by the recent work of Petters, Blosser, and Hereford.[11] Although the Bethe formula has never been found to be incorrect, it has not been checked accurately for low electron energies. The most recent measurements have been made by Kageyama and Nishimura[12] who found agreement within a few percent for the average stopping power of electrons in the range from 600 kev to 1.76 Mev.

The experimental error was computed on the basis of a probable error of 1% in the chamber depth and a probable error in the slope of the incremental ion current vs pressure as computed below for each point. Errors due to variations in temperature (the room was air conditioned) and foil thickness (weighed on an analytical balance and gauged on a Pratt and

---

[11] W. G. Petters, H. G. Blosser, and F. L. Hereford, Phys. Rev. 101, 17 (1956).

[12] Seizaburo Kageyama and Kazuaka Nishimura, J. Phys. Soc. Jap. 7, 292 (1952).

Whitney Electrolimit gauge) were considered as negligible. Errors due to reading pressures and meters are reflected in the probable error assigned to the slope, a. The W value of air for electrons of 34.0 ev/i.p. given by Jesse and Sadauskis[13] was used and no probable error was assigned for its accuracy or its variation (if any) with energy.

The slope of a line through the five points was given a conventional least squares fit[14] for each foil at each energy for both positive and negative collection potentials. Assuming the form,

$$y = ax + b$$

$$a = \frac{n\sum x_i y_i - \sum x_i \sum y_i}{n\sum x_i^2 - \left(\sum x_i\right)^2}$$

$$PE_a = \sqrt{\frac{n}{n\sum x_i^2 - \left(\sum x_i\right)^2}}\; PE_y$$

$$PE_y = \sqrt{\frac{\sum (\delta y_i)^2}{n - 1}}\,(0.675)$$

$$\sum(\delta y_i)^2 = \sum y_i^2 - 2a\sum y_i - 2b\sum x_i y_i + na^2 + 2ab\sum x_i + b^2\sum x_i^2$$

---

13 W. P. Jesse and J. Sadauskis, Phys. Rev. 97, 1668 (1955).

14 Worthing and Geffner, TREATMENT OF EXPERIMENTAL DATA, p 249, John Wiley and Sons, New York, 1943.

This requires the computation

$$b = \frac{\sum x_i^2 \sum y_i - \sum x_i \sum x_i y_i}{n \sum x_i^2 - \left(\sum x_i\right)^2}$$

The positive a and negative a were averaged to give $\bar{a}$.

$$PE_{\bar{a}} = \sqrt{(PE_{pos\ a})^2 + (PE_{neg\ a})^2}$$

$$PE_{total} = \sqrt{(PE_{\bar{a}})^2 + (PE_{depth})^2}$$

Probable errors were computed for each point by this procedure and are shown in Figs. 3, 4, 5, and 6.

VII. COMPARISON OF EXPERIMENT WITH THEORY

The data taken at 126.5, 104, 80, and 57 kev were compared with adjusted theoretical curves calculated at 125, 100, 75, and 50 kev, respectively, and the results are shown in Figs. 6, 5, 4, and 3. The theoretical curves were adjusted by multiplying the theoretical ordinate by the ratio of energy of data to energy of the calculation, i.e., 126.5/125, etc. This procedure appears to be justified because of the striking independence of curve shape on the incident energy. There is

good agreement between calculated and experimental values except near the source plane x = 0 and in the tail on the positive side. The experimental curve crosses the theoretical curve three times in every case.

For an additional comparison the theoretical curves were normalized by dividing the ordinates by the incident energy in kev. The results shown in Fig. 21 for our normalized 50, 75, 100, and 125 kev theoretical distributions together with Spencer's 500 kev distribution suggest that some universal curve might exist over a limited range.

Another comparison is shown in Fig. 22 for which the normalized experimental points are compared with an average curve of the four normalized distributions (50, 75, 100, and 125 kev) shown in Fig. 21. Apparently the experimental data agree better with Spencer's normalized 500 kev distribution in Fig. 21 than with our own average curve. The experimental data consistently start lower than our theoretical calculation, peak slightly higher and at a smaller x than the theory, drop below the theory on the backside of the distribution, and again rise above the theory for deep penetration. It is noteworthy that the areas of the experimental and theoretical curves are approximately the same. The drop near the source plane might be caused by loss of backscattered electrons through the window although the small solid angle subtended by the window for this process should have minimized this effect. In the positive tail, range straggling effects not included in the present theory should increase the experimental ionization over that predicted

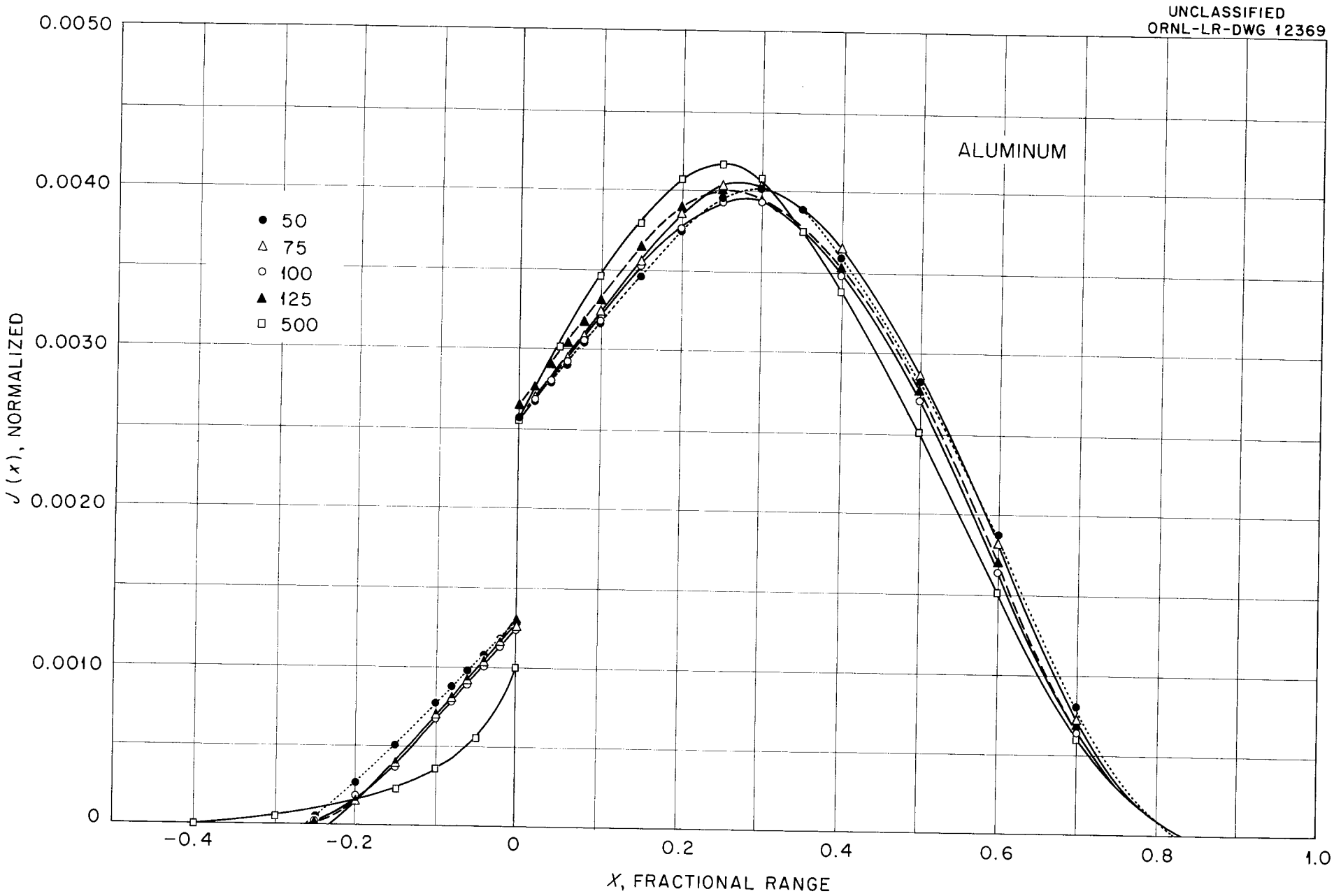

FIG. 21
NORMALIZED, THEORETICAL, SPATIAL DISTRIBUTIONS AS A FUNCTION OF PENETRATION DEPTH

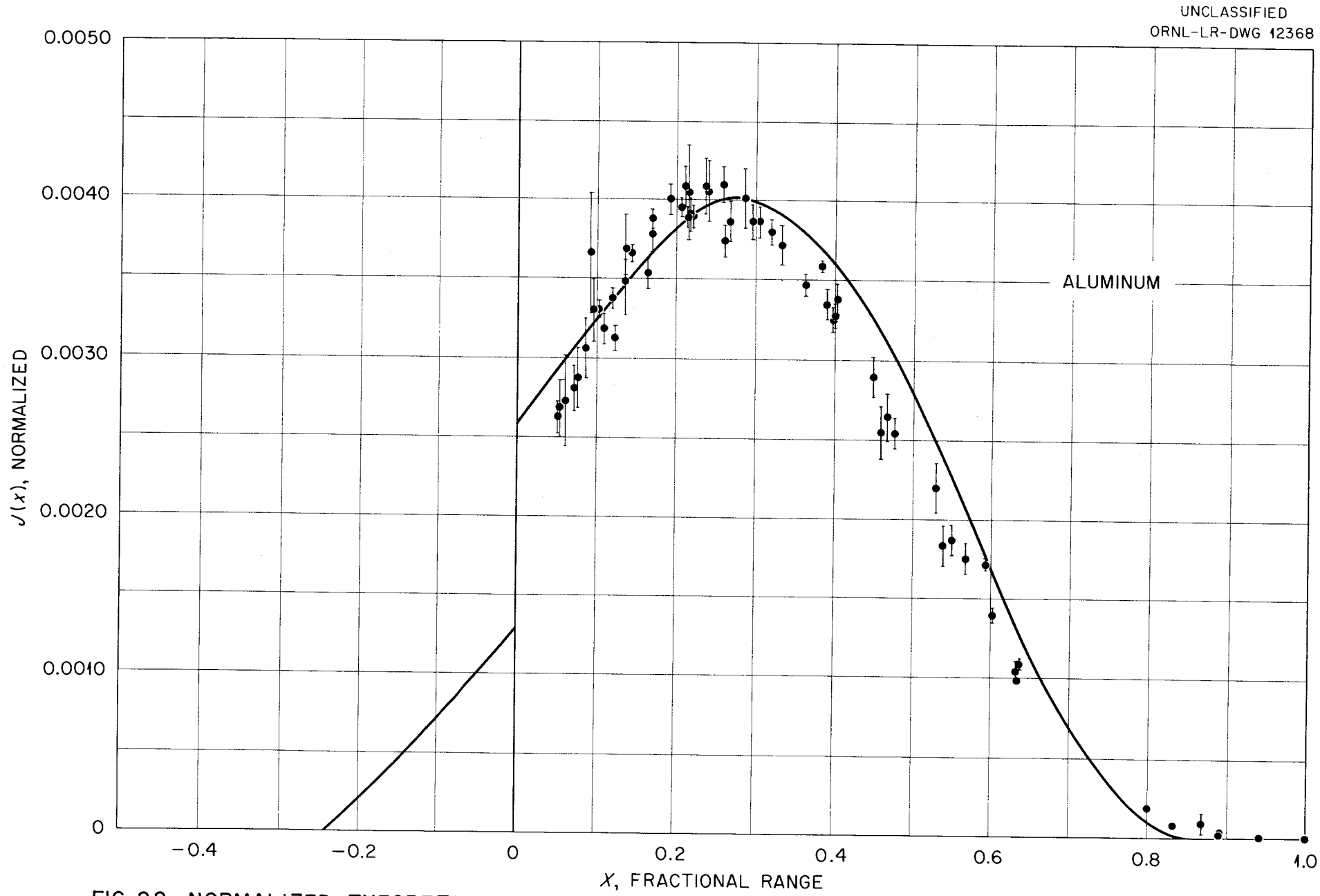

FIG. 22 NORMALIZED, THEORETICAL, SPATIAL DISTRIBUTIONS AS A FUNCTION OF PENETRATION DEPTH. POINTS ARE NORMALIZED EXPERIMENTAL VALUES AND SOLID LINE IS NORMALIZED SPENCER THEORY.

by theory.

Although most of the points agree with the normalized distribution within their probable error, the consistency of the data would indicate that our calculations of the Spencer theory differ slightly from the experimental observations.

VIII. COMPARISON WITH OTHER EXPERIMENTS

The rate at which a monoenergetic beam of electrons dissipates energy when normally incident on a slab of material has been experimentally investigated a number of times, originally because of the importance of such information to biologists and radiologists in estimating electron beam dosages, and later to physicists who were interested in the problem from a theoretical standpoint. The general shape of the curves was first determined by Trump, Van de Graaff, and Cloud[15] at incident energies from 300 kev to 1500 kev for absorbers of water, Al, Cu, and Pb. The procedure involved the introduction of a parallel plate ionization chamber behind the various absorbing foils, with the resulting ion current then being a measure of the amount of energy left behind in the medium at that depth provided that the value of W, the average energy required to form an ion pair, could be considered to be independent of the electron energy. Several experimental problems become apparent as a result of this early work. Ideally both

---

[15] J. G. Trump, R. J. Van de Graaff, and R. W. Cloud, Amer. J. Roent. 43, 728 (1940).

the absorbing material and the back of the ion chamber should be of the same material, with the latter of thickness greater than the range of the primary beam. The filling gas should be of the same or nearly the same atomic number as the absorbing material and the chamber should have lateral dimensions as large as the range of the electrons in the gas. Also, the electrons backscattered from the surface of the foil should be considered, especially where absolute measurements of energy dissipation are involved.

In the experiments of Trump, Van de Graaff, and Cloud, a steel plate was used at the exit face of the ion chamber regardless of the composition of the absorbing foils. Thus backscatter into the chamber could be expected to be different from that arising in an infinite homogeneous slab. However, subsequent experiments[16] yielded curves of energy dissipation in aluminum which have quantitative significance. These are reproduced in Fig. 23 for energies of 2 Mev and 3 Mev, with the data taken by Frantz at 515 kev and the present data at 126.5 and 57 kev. Distributions constructed from the Spencer theory are plotted for 500, 126.5, and 57 kev beams on aluminum, so that this figure outlines the available data and theory on the depth dose of electrons in aluminum.

IX. SUMMARY OF FINDINGS AND CONCLUSIONS

The findings are best summarized by Fig. 22. There seems to be

---

16 J. G. Trump, K. A. Wright, and A. M. Clarke, J. Appl. Phys. 21, 345 (1950).

ORNL-LR-Dwg. 13849
UNCLASSIFIED

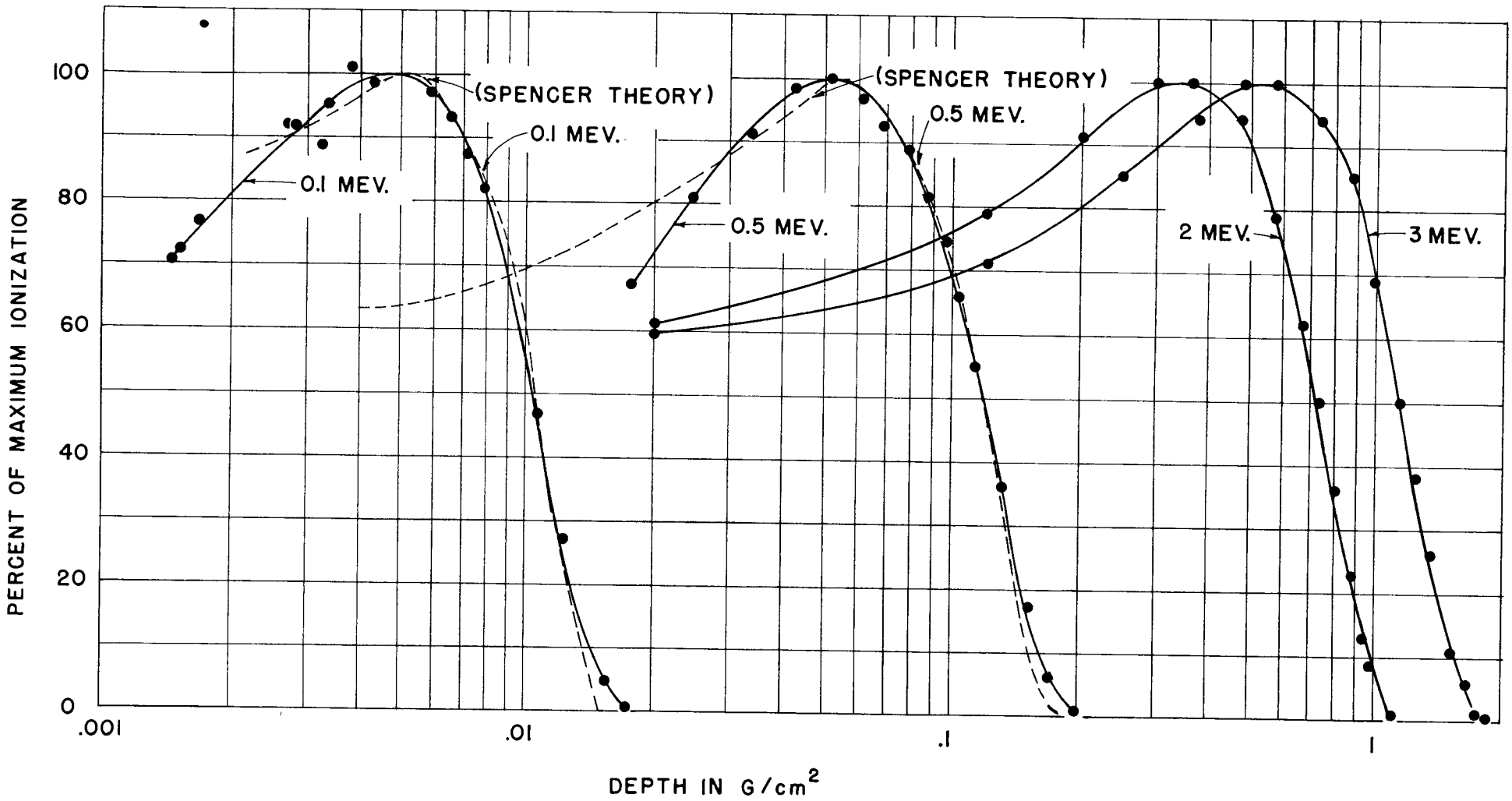

FIG. 23- PERCENT MAXIMUM IONIZATION VS. DEPTH IN g/cm² ALUMINUM CURVES

a small, but definite, discrepancy between theory and experiment although the theory lies within the probable error in most cases.

It is beyond the scope of this paper to explain this discrepancy although several possibilities present themselves. The reliability of the Mott theory and the Bethe formula as well as the accuracy of the Spencer moment fitting method have already been discussed. There may be something fundamentally incorrect with the experimental arrangement and treatment of the data. Alternatively, because our data agree with the normalized Spencer distribution for 500 kev better than the distributions given here, one would suspect that our theoretical distributions are somewhat incorrect.

BIBLIOGRAPHY

Beers, Y., THEORY OF ERROR, Cambridge: Addison-Wesley, 1953.

Bethe, H. A., HANDBUCH DER PHYSIK 24, Part 1, p 491, Berlin: Verlag Julius Springer, 1933.

Blackstock, A. W., Birkhoff, R. D., and Slater, M., "Electron Accelerator and High Resolution Analyzer," Rev. Sci. Instr. 26, 274 (1955).

Fano, U., "Inelastic Collisions and the Molière Theory of Multiple Scattering," Phys. Rev. 93, 117 (1954).

Jesse, W. P. and Sadauskis, J., "Ionization in Pure Gases and the Average Energy to Make an Ion Pair for Alpha and Beta Particles," Phys. Rev. 97, 1668 (1955).

Kageyama, Seizaburo, and Nishimura, Kazuaka, "On the Energy Loss of Fast Electrons," J. Phys. Soc. Jap. 7, 292 (1952).

Lewis, H. W., "Multiple Scattering in an Infinite Medium," Phys. Rev. 78, 576 (1950).

National Bureau of Standards, "Tables of Sine, Cosine, and Exponential Integrals," TABLES, Washington: Government Printing Office, 1940.

Petters, W. G., Blosser, H. G., and Hereford, F. L., "Scattering of 200 kev Electrons in Gold," Phys. Rev. 101, 17 (1956).

Spencer, L. V., "Penetration and Diffusion of X Rays: Calculation of Spatial Distributions by Semi-Asymptotic Methods," Phys. Rev. 88, 793 (1952).

Spencer, L. V., "Theory of Electron Penetration," Phys. Rev. 98, 1597 (1955).

Trump, J. G., Van de Graaff, R. J., and Cloud, R. W., "Cathode Rays for Radiation Therapy," Amer. J. Roent. 43, 728 (1940).

Trump, J. G., Wright, K. A., and Clarke, A. M., "Distribution of Ionization in Materials Irradiated by Two and Three Million-Volt Cathode Rays," J. Appl. Phys. 21, 345 (1950).

Watson, G. N., "Theory of Bessel Functions," TABLES, Cambridge: Cambridge University Press, 1952.

Wick, G. C., "On the Space Distribution of Slow Neutrons," Phys. Rev. 75, 783 (1949).

Worthing, A. G., and Geffner, J., TREATMENT OF EXPERIMENTAL DATA, New York: John Wiley and Sons, 1943.

ACKNOWLEDGMENTS

The author wishes to express sincere gratitude to Dr. R. D. Birkhoff, Oak Ridge National Laboratory, who suggested and supervised this thesis. Also, he expresses his appreciation to L. V. Spencer and U. Fano of the National Bureau of Standards for suggestions on the ionization chamber design and aid in constructing the theoretical distributions. He thanks J. S. Cheka for aid in the calculations and B. G. Saunders for help with the experimental data.

An AEC Radiological Physics Fellowship enabled the author to pursue this study.